Manuscript prepared for Geosci. Model Dev.
with version 2014/07/29 7.12 Copernicus papers of the LaTeX class copernicus.cls.
Date: 23 June 2017

OMEN-SED 1.0: A new, numerically efficient sediment module for the coupling to Earth System Models

Dominik Hülse[1], Sandra Arndt[1, 2], Stuart Daines[3], Andy Ridgwell[1, 4], and Pierre Regnier[2]

[1]School of Geographical Sciences, University of Bristol, Clifton, Bristol BS8 1SS, UK
[2]Department of Earth and Environmental Sciences, Université Libre de Bruxelles, Brussels, Belgium
[3]Earth System Science, University of Exeter, North Park Road, Exeter EX4 4QE, UK
[4]Department of Earth Sciences, University of California, Riverside, CA 92521, USA

Correspondence to: Dominik Hülse (Dominik.Huelse@bristol.ac.uk)

Abstract. Here we describe the first version of a new, analytical early diagenetic model resolving organic matter cycling and associated biogeochemical dynamics in marine sediments called OMEN-SED (Organic Matter ENabled SEDiment model). Most biogeochemical cycles and reactions in the surface sediments can be related either directly or indirectly to the degradation of organic matter. Despite its fundamental importance, an appropriate Earth System model of the coupled atmosphere-ocean-sediment system which is able to model all relevant processes and feedbacks over geological time-scales currently does not exist. The major problem is the high computational cost of simulating the essential redox reactions in marine sediments which are important to calculate burial of organic matter and benthic recycling fluxes of chemical compounds. In most Earth System models sediment-water dynamics are either neglected or treated in a very simplistic way. To provide a more realistic description of organic matter degradation and nutrient cycles in marine sediments we have developed OMEN-SED, a new, one-dimensional, numerically efficient reactive transport model. OMEN-SED is the first analytical model to explicitly describe organic matter cycling as well as associated dynamics of the most important terminal electron acceptors (i.e. O2 , NO3, SO4), related reduced substances (NH4, H2S), the full suite of secondary-redox reactions, macronutrients (PO4) and associated pore water quantities (ALK, DIC). To represent a redox-dependent sedimentary P cycle we consider the formation and burial of Fe-bound P and authigenic Ca-P minerals. Thus, OMEN-SED captures most of the features of a complex, numerical diagenetic model, however, its computational efficiency allows the coupling to global Earth System models and therefore the investigation of coupled global biogeochemical dynamics over different timescales. This paper provides a detailed description of

the new sediment model, tested with observations, SA and global observations and describes it's coupling to the Earth System model cGENIE.

Contents

1 Introduction

DH: Will delete the sub-headings!

Role of marine sediments for climate and global biogeochemical cycles:

Marine surface sediments are key components in the Earth system. They host the largest carbon reservoir within the surficial Earth system, provide the only long term sink for atmospheric CO_2, recycle nutrients and represent the most important geochemical archive used for deciphering past changes in biogeochemical cycles and climate (e.g. Berner, 1991; Archer and Maier-Reimer, 1994; Ridgwell and Zeebe, 2005; Arndt et al., 2013). Physical and chemical processes in sediments (i.e. diagenetic processes) depend on the water column and vice versa: Diagenesis is mainly donor controlled, as it is fuelled by the external supply of solid material (e.g. organic matter, calcium carbonate, opal) from the water column and is affected by overlying bottom water concentrations of solutes. At the same time, sediments impact the water column directly either by short- and long-term storage of deposited material or diagenesis transforms deposited material and returns some of the resulting products (e.g. nutrients, DIC) to the bottom waters. This so-called benthic-pelagic coupling is essential for understanding global biogeochemical cycles and climate (e.g. Archer and Maier-Reimer, 1994; Archer et al., 2000; Soetaert et al., 2000; Mackenzie, 2005).

Biological primary production of organic matter (OM, CH_2O in equation R1) and the reverse process of degradation can be written in a greatly simplified reaction as:

$$CO_2 + H_2O \rightleftharpoons CH_2O + O_2. \quad \text{(R1)}$$

On geological timescales production of OM is generally greater than degradation which results in some organic matter being buried in marine sediments and oxygen accumulating in the atmosphere. Thus burial of OM leads to net oxygen input to, and CO_2 removal from the atmosphere (Berner, 2004). On shorter timescales, the upper few meters of the sediments (i.e. early diagenesis) are specifically important as it is decided here if a substance is recycled to the water column or buried for a longer period of time in the deeper sediments (Hensen et al., 2006). Most biogeochemical cycles and reactions in this part of marine sediments can be related either directly or indirectly to the degradation of organic matter (e.g Boudreau and Ruddick, 1991; Arndt et al., 2013). Organic matter degradation releases metabolic CO_2 to the pore water, causing it to have a lower pH and provoking the dissolution of $CaCO_3$ (Emerson and Bender, 1981). Oxygen and nitrate for instance, the most powerful electron acceptors, are consumed in the course of the degradation of organic matter, resulting in the release of ammonium and phosphorous to the pore water. As such, degradation of OM in the sediments can profoundly affect the oxygen and nutrient inventory of the ocean and thus primary productivity (Van Cappellen and Ingall, 1994; Lenton and Watson, 2000).

Nutrient recycling from marine sediments has been suggested to play a key role for climate and ocean biogeochemistry for different events during Earth history. For example, feedbacks between phosphorous storage and erosion from shelf sediments and marine productivity have been hypothesised to play an important role for glacial/interglacial atmospheric CO_2 changes (Broecker, 1982;

Ruttenberg, 1993). Furthermore, nutrient recycling from anoxic sediments has been invoked to explain the occurance of more extreme events in Earth history, for instance Oceanic Anoxic Events (OAEs, e.g. Mort et al., 2007; Tsandev and Slomp, 2009). OAEs represent severe disturbances of the global carbon, oxygen and nutrient cycles of the ocean and are usually characterized by widespread bottom water anoxia and photic zone euxinia (Jenkyns, 2010). One way to explain the genesis and persistence of OAEs is increased oxygen demand due to enhanced primary productivity. Increased nutrient inputs to fuel primary productivity may have come from marine sediments as the burial efficiency of phosphorus declines when bottom waters become anoxic (Ingall and Jahnke, 1994; Van Cappellen and Ingall, 1994). The recovery from OAE like conditions is thought to involve the permanent removal of excess CO_2 from the atmosphere and ocean by burying carbon in the form of organic matter in marine sediments (e.g. Arthur et al., 1988; Jarvis et al., 2011), which is consistent with the geological record of widespread black shale formation (Stein et al., 1986). However, the overall amount, exact timing and the rate of organic matter burial remain a topic of an ongoing debate.

Diagenetic Models:

Therefore, globally quantifying the burial and degradation of organic matter in marine sediments and related biogeochemical dynamics is important for understanding climate and the cycling of many chemical elements on various timescales. Such studies and quantifications are possible through the application of idealised mathematical representations of diagenesis, or so-called diagenetic models (see e.g. Berner, 1980; Boudreau, 1997). The number of research questions that can be addressed with diagenetic models is infinite and a plethora of different approaches have been developed, mainly following two distinct directions (Arndt et al., 2013).

First, state-of-the art vertically resolved numerical models simulating the entire suite of essential coupled redox and equilibrium reactions within marine sediments (e.g. BRNS, Aguilera et al., 2005; CANDI, Boudreau, 1996; MEDIA, Meysman et al., 2003; STEADYSED, Van Cappellen and Wang, 1996). These "complete", non-steady-state models, thus resolve the resulting characteristic redox-zonation of marine sediments through explicitly including oxic OM degradation, denitrification, oxidation by manganese and iron (hydr)oxides, sulfate reduction and methanogenesis as well as the reoxidation of reduced byproducts (i.e. NH_4, Mn^{2+}, Fe^{2+}, H_2S, CH_4). Furthermore, they incorporate various mineral dissolution and precipitation reactions, as well as fast equilibrium sorption processes for example of NH_4, PO_4 and metal ions (i.e. Mn^{2+}, Fe^{2+} and Mg^{2+}, compare Van Cappellen and Wang, 1996; Meysman et al., 2003). Modelled, depth-dependent, transport processes usually comprise advection, diffusion, bioturbation and bio-irrigation. This group of diagenetic models generally uses a so-called multi-G approach (Jørgensen, 1978; Berner, 1980), thus dividing the bulk organic matter pool into a number of compound classes that are characterised by different degradabilities k_i, which are generally dependent on the type and concentration of the specific terminal electron acceptor (TEA). These complex models have a great potential for quantifying OM degra-

dation dynamics for sites where enough observations are available to constrain its model parameters (see e.g. Boudreau et al., 1998; Wang and Van Cappellen, 1996; Thullner et al., 2009, for applications). However, due to the high degree of coupled processes and depth-varying parameters the diagenetic equation needs to be solved numerically, thus resulting in a very high computational demand and consequently rendering their application in an Earth system model framework prohibitive. Additionally, their global applicability is limited by the restricted transferability of model parameters from one site to the global scale (Arndt et al., 2013).

The second group of models solves the diagenetic equation analytically or semi-analytically, thus providing an alternative and computational more efficient approach. However, finding an analytical solution, especially when complex reaction networks are to be considered, is not straightforward and generally requires the assumption of steady state. The complexity of the reaction network can be reduced by dividing the sediment column into distinct zones and accounting for the most pertinent biogeochemical processes within each zone, thus increasing the likelihood of finding an analytical solution. In general, analytical diagenetic models are less sophisticated and comprehensive than numerical models and are used for the coupling to global ESMs (e.g. HAMOCC and NorESM use the model of Heinze et al. (1999)) or box models (e.g. DCESS, Shaffer et al., 2008 or MBM using MEDUSA, Munhoven, 2007). These analytic or semi-analytical models account for the most important transport processes (i.e advection, bioturbation and molecular diffusion) through basic parametrizations and include fewer biogeochemical reactions which are generally restricted to the upper, bioturbated 10 cm of the sediments. They assume that the sedimentary organic matter pool is composed of just a single compound class which is either degraded with a globally invariant degradation rate constant (Munhoven, 2007) or a fixed rate constant depending on local oxygen concentrations (Shaffer et al., 2008; Palastanga et al., 2011). Pore water tracers explicitly represented in DCESS (Shaffer et al., 2008) and the HAMOCC model of Heinze et al. (1999) and Palastanga et al. (2011) are restricted to DIC, TA, PO_4 and O_2. The MEDUSA model (Munhoven, 2007) considers CO_2, HCO_3^-, CO_3^{2-} and O_2. Other species produced or consumed during OM degradation are neglected. Thus, with oxygen being the only TEA explicitly modelled the influence of reduced species is only implicitly included in the boundary conditions for O_2. A newer versions of the HAMOCC model, being a notable exception, as Ilyina et al. (2013) include NO_3 and denitrification explicitly. Furthermore, the version of Palastanga et al. (2011) represents an redox-dependent explicit sedimentary phosphorus cycle. Yet, secondary redox reactions involving reduced substances or sorption processes are not included in any of the discussed models.

How are sediments resolved in Earth system models:

Earth system models generally track the biogeochemical dynamics of organic and inorganic carbon, essential nutrients (nitrogen, phosphorus) and oxygen with the aim of investigating the evolution of the ocean's redox structure and carbonate system and its feedbacks on global climate. This general aim thus defines a minimum set of state variables and reaction processes that need to be resolved

for an efficient representation of the benthic-pelagic coupling in Earth system models. A suitable sediment model has to provide a robust quantification of organic (and inorganic) carbon burial fluxes, as well as benthic uptake/return fluxes of oxygen, growth-limiting nutrients and reduced species. As a consequence, the reaction network must account for the most important primary and secondary redox reactions, equilibrium reactions, mineral precipitation/dissolution and adsorption/desorption, resulting in a complex set of coupled reaction-transport equations.

Even though there are more appropriate sediment representations, in most current ESMs sediment-water dynamics are either neglected or treated in a very simplistic way (Soetaert et al., 2000; Hülse et al., 2017). Most Earth system Models of Intermediate Complexity (EMICs) and also some of the higher resolution global carbon cycle models represent the sediment-water interface either as a reflective or a conservative/semi-reflective boundary (Hülse et al., 2017). Thus, all particulate material deposited on the seafloor is either instantaneously consumed (reflective boundary), or a fixed fraction is buried in the sediments (conservative/semi-reflective boundary). Both highly simplified approaches furthermore completely neglect the exchange of solute species through the sediment-water interface and, therefore, cannot resolve the complex benthic-pelagic coupling. However, due to their computational efficiency, both representations are often used in global biogeochemical models (e.g. Najjar et al., 2007; Ridgwell et al., 2007; Goosse et al., 2010). A superior approach is the vertically integrated dynamic model, which represents the whole sediment column as a single box (Hülse et al., 2017). Here, OM deposited on the seafloor is added to the sediment box where it gets degraded and dissolved species diffuse through the sediment-water interface in accordance with these transformations. This approach thus ignores the vertical extent of the sediments and the temporary storage of dissolved species (Soetaert et al., 2000). Yet, it is computationally efficient and allows differentiating between various fractions of organic matter. Most EMICs incorporate a vertically integrated dynamic model for particulate inorganic carbon only (i.e. mainly $\mathrm{CaCO_3}$) and just a few consider oxic-only sediment degradation of organic matter (Hülse et al., 2017).

The most complex description of diagenetic organic matter degradation in Earth system models is the second group of vertically resolved diagenetic models as discussed above (e.g. Heinze et al., 1999; Munhoven, 2007; Shaffer et al., 2008). These models solve the one-dimensional reaction-transport equation for a number of solid and dissolved species for the upper, bioturbated 10 cm of the sediments. Examples of global ESMs employing a vertically resolved diagenetic model are NorESM (Tjiputra et al., 2013) and HAMOCC (Palastanga et al., 2011; Ilyina et al., 2013), both using a version of Heinze et al. (1999). None of the EMICs reviewed by Hülse et al. (2017) use such a sediment representation. DCESS (Shaffer et al., 2008) and MBM (Munhoven, 2007) are box models employing a vertically resolved diagenetic model. However, in general oxygen is the only TEA explicitly modelled and secondary redox reactions and reduced species are completely neglected in these approaches. Furthermore, all models represent the bulk OM pool as a single fraction with a fixed degradation rate constant.

Problem with that:

Obviously, such a simplification of the OM pool can neither account for the observed vast structural complexity in natural organic matter and its resulting different degradation rates nor for the rapid decrease in OM degradability in the uppermost centimetres of the sediments (Arndt et al., 2013). It has been suggested that at least a 3G approach is necessary to accurately represent organic matter dynamics in this part of the sediments where most OM is degraded (e.g. Soetaert et al., 1996b). Even more restrictive is the use of O_2 as the only TEA and the complete absence of reduced substances and related secondary redox reactions. Even though for the majority of the modern sediments (i.e. in the deep-ocean) O_2 is the primary electron acceptor and Archer et al. (2002) suggested that aerobic degradation accounts for 66% of total organic matter respiration more recent model and data studies have reported that sulfate reduction is the dominant degradation pathway on a global average (with contributions of 55-76% Canfield et al., 2005; Jørgensen and Kasten, 2006; Thullner et al., 2009). O_2 becomes progressively less important as TEA with decreasing seafloor depth and in shallow waters most of it is used to reoxidise reduced substances produced during anaerobic degradation (Canfield et al., 2005; Thullner et al., 2009). Thus, the in situ production of e.g. NO_3 and SO_4 through oxidation of NH_4 and H_2S forms an important sink for O_2 which is entirely neglected in current sediment representations in global models. In addition, due to the lack of an appropriate sedimentary P cycle (with the exception of the HAMOCC version of Palastanga et al. (2011), no current global ESM is able to model the redox dependent P release from marine sediments and its implications for primary productivity, global biogeochemical cycles and climate.

Solution presented here:

In order to provide a more realistic description of organic matter degradation and nutrient cycles in marine sediments we have developed the OrganicMatter ENabled SEDiment model (OMEN-SED), a new, one-dimensional, numerically efficient reactive transport model. OMEN-SED is the first analytical model to explicitly describe OM cycling as well as associated dynamics of the most important TEAs (i.e. O_2, NO_3, SO_4), related reduced substances (NH_4, H_2S), the full suite of secondary-redox reactions, macronutrients (PO_4) and associated pore water quantities (ALK, DIC). To represent a redox-dependent sedimentary P cycle we consider the formation and burial of Fe-bound P and authigenic Ca-P minerals. Thus, OMEN-SED captures most of the features of a complex, numerical diagenetic model, however, its computational efficiency allows the coupling to global Earth system models and therefore the investigation of coupled global biogeochemical dynamics over different timescales. Here, the model is presented as a 2G-approach, however, a third, non-degradable OM fraction can easily be added and OMEN-SED can be further extended to a Multi-G approach.

SA: started here

general notes:

-name zones I and II bio and non-bio

-name redox zones according to Canfield paper

- be consistent in the paper and always use the same terminology e.g. zone, boundary,...
- don't use I and II for the bioturb, non-bioturb zones and the redox zones. For the redox zones, you actually do not need to use I, II, and III at all, because you name the zone explicitly, so this should be clear

DH: Not 100% sure about redox zones: I don't use suboxic anymore (Canfield and Thamdrup, 2009), and just use anoxic when referring to all zones $z < z_{\mathrm{ox}}$ together, defined in Sec. 2.2.2)??

2 Model Description

OMEN-SED a new, one-dimensional, computationally efficient reaction-transport model is designed for the coupling to regional/global biogeochemical and Earth system models. OMEN-SED is implemented as a Fortran version that can be easily coupled to a pelagic model via the coupling routine **OMEN_SED_main**. In addition, OMEN-SED exists as a stand-alone version implemented in MATLAB and the complete model can be executed on a standard personal computer in less than 0.1 seconds. The source code of both, the Fortran and the MATLAB stand-alone version, as well as instructions for executing OMEN-SED and plotting results **TODO (maybe include some examples and test figures?)** are available as a supplement to this paper. The following section provides a detailed description of OMEN-SED. Table 1 summarises the biogeochemical reaction network and a glossary of model parameters along with their respective units is provided in Tables 9 and 10.

2.1 General Model Approach

The calculation of benthic uptake, recycling and burial fluxes is based on the vertically resolved conservation equation for solid and dissolved species in porous media (e.g. Berner, 1980; Boudreau, 1997):

$$\frac{\partial \xi C_i}{\partial t} = -\frac{\partial F}{\partial z} + \xi \sum_j R_i^j \tag{1}$$

where C_i is the concentration of biogeochemical species i, ξ equals the porosity ϕ for solute species and $(1-\phi)$ for solid species. The term z is the sediment depth, t denotes the time, F summarises the transport fluxes and $\sum_j R_i^j$ represents the sum of all biogeochemical rates j affecting species i.

OMEN-SED accounts for both the advective, as well as the diffusive transport of dissolved and solid species. Solid and dissolved species are buried in the sediment according to a constant burial rate w, thus neglecting the effect of sediment compaction (i.e. $\frac{\partial \phi}{\partial z} = 0$) due to mathematical constraints. The molecular diffusion of dissolved species is described by Fick's law applying a species-specific apparent diffusion coefficient, $D_{\mathrm{mol},i}$. In addition, the activity of infaunal organisms in the bioturbated zone is simulated using a diffusive term (e.g. Boudreau,1986), with a constant bioturbation coefficient D_{bio} in the bioturbated zone, while D_{bio} is set to zero below z_{bio}. The pumping activity by burrow-dwelling animals and the resulting ventilation of tubes, the so-called bioirri-

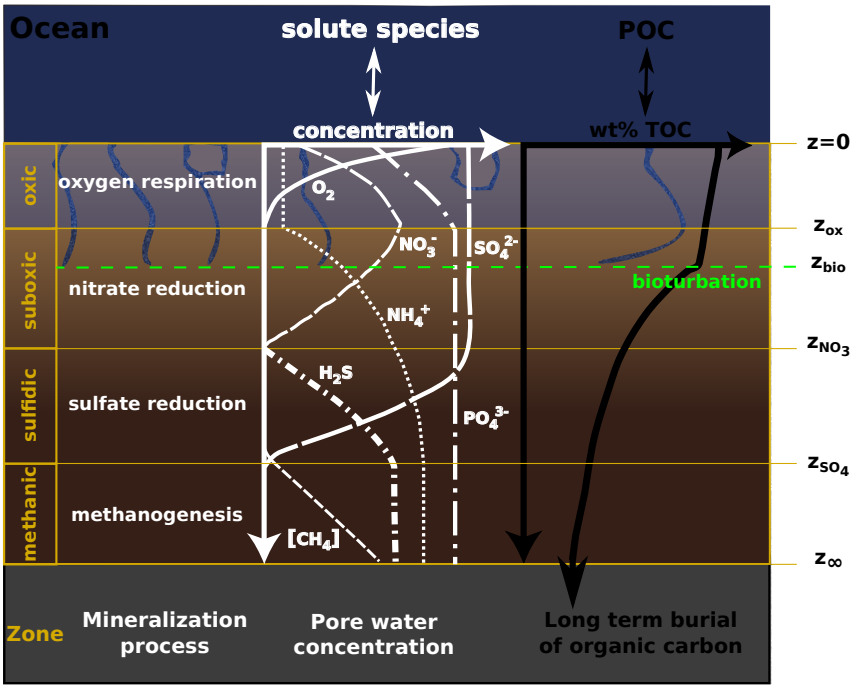

Figure 1. Schematic of the different modelled species and layers in OMEN-SED. Here showing the case $z_{\mathrm{ox}} < z_{\mathrm{bio}} < z_{\mathrm{NO_3}} < z_{\mathrm{SO_4}}$.

gation, is encapsulated in a factor, f_{ir} that enhances the molecular diffusion coefficient (hence, $D_{i,0} = D_{\mathrm{mol},i} \cdot f_{ir}$, Soetaert et al., 1996a). The flux divergence is thus given by:

$$\frac{\partial F}{\partial z} = -\frac{\partial}{\partial z}\left(-\xi D_i \frac{\partial C_i}{\partial z} + \xi w C_i\right) \tag{2}$$

where D_i is the apparent diffusion coefficient of species i ($D_i = D_{i,0} + D_{\mathrm{bio}} = D_{\mathrm{mol},i} \cdot f_{ir} + D_{\mathrm{bio}}$ for dissolved species and $D_i = D_{\mathrm{bio}}$ for solid species) and w is the burial rate.

The reaction network of OMEN-SED accounts for the most important primary and secondary redox reactions, equilibrium reactions, mineral dissolution and precipitation, as well as adsorption and desorption processes that affect the dissolved and solid species explicitly resolved in OMEN-SED. Table 1 provides a summary of the reactions and biogeochemical tracers considered in OMEN-SED. **SA: Tab 1 is maybe a bit redundant? DH: I still think it's a good summary/overview!?** Table 15 summarises their reaction stoichiometry and Table **??** provides an overview of their description in the model.

Based on Eq. (1), OMEN-SED calculates the fraction of POC buried in the sediment, f_{POC}, as well as the benthic uptake/return fluxes F_{C_i} of dissolved species C_i (in mol cm^{-2} year^{-1}) in response to changing boundary conditions and forcings:

Table 1. Reactions and biogeochemical tracers implemented in the reaction network of OMEN-SED. The primary and secondary redox reactions are listed in the sequence they occur with increasing sediment depth.

	Description
Primary redox reactions	Degradation of organic matter via aerobic degradation, denitrification, sulfate reduction, methanogenesis (implicit)
Secondary redox reactions	Oxidation of ammonium and sulfide by oxygen, anaerobic oxidation of methane by sulfate
Adsorption/Desorption	Ad-/Desorption of P on/from $\mathrm{Fe(OH)_3}$, $\mathrm{NH_4}$ adsorption, $\mathrm{PO_4}$ adsorption
Mineral precipitation	Formation of authigenic P
Biogeochemical tracers	Organic matter (2-G), oxygen, nitrate, ammonium, sulfate, sulfide (hydrogen sulfide), phosphate, Fe-bound P, DIC, ALK

$$f_{\mathrm{POC}} = \frac{\mathrm{POC}(z_\infty)}{\mathrm{POC}(0)} \tag{3}$$

$$F_{C_i} = \phi(0)\left(D_i \frac{\partial C_i(z)}{\partial z}\bigg|_{z=0} - w\left[C_i(0) - C_i(z_\infty)\right]\right) \tag{4}$$

where w is the deposition rate, D_i is the diffusion coefficient and $\mathrm{POC}(0)$, $\mathrm{POC}(z_\infty)$, $C_i(0)$, $C_i(z_\infty)$ denotes the concentration of POC and dissolved species i at the SWI and at the lower sediment boundary, respectively.

Because OMEN-SED is designed for application in Earth System Models it requires a computationally efficient solution of Eq. (1) and, thus, solves Eq. (1) analytically, by assuming steady state conditions (i.e. $\frac{\partial C_i}{\partial t} = 0$) and dividing the sediment column into a number of different zones (Fig. 1). Each of these zones is characterised by a different set of equations that encapsulate the most pertinent reaction and transport processes within the respective zone (see Section 2.2 for more details), thus allowing a simplification of the coupled set of equations. More specifically, OMEN-SED divides the sediment column into I) a bioturbated and II) a non-bioturbated zone defined by an imposed, constant bioturbation depth z_{bio} (see Fig. 1). Furthermore, it resolves the dynamic redox stratification of marine sediments by dividing the sediment into 1) an oxic zone delineated by the oxygen penetration depth z_{ox}; 2) a denitrification zone situated between z_{ox} and the nitrate penetration depth $z_{\mathrm{NO_3}}$; 3) a sulfate reduction zone situated between $z_{\mathrm{NO_3}}$ and the sulfate penetration depth $z_{\mathrm{SO_4}}$; and 4) a methanogenic zone situated below $z_{\mathrm{SO_4}}$ (Fig. 1). All penetration depths are dynamically calculated by the model and their depth thus varies in response to changing boundary conditions and forcings.

2.2 Conservation Equations and Analytical Solution

2.2.1 Organic matter or Particulate Organic Carbon (POC)

In marine sediments, organic matter (OM) is degraded by heterotrophic activity coupled to the sequential utilisation of terminal electron acceptors according to the free energy gain of the half-reaction ($O_2 > NO_3^- > MnO_2 > Fe(OH)_3 > SO_4^{2-}$, e.g. Stumm and Morgan, 2012). Here, organic matter degradation is described via a multi G-model approach (Arndt et al., 2013, and references therein), dividing the bulk OM into a number i of discrete compound classes C_i characterised by class-specific first-order degradation rate constants k_i. The conservation equation for organic matter dynamics is thus given by:

$$\frac{\partial C_i}{\partial t} = 0 = D_{C_i}\frac{\partial^2 C_i}{\partial z^2} - w\frac{\partial C_i}{\partial z} - k_i \cdot C_i \tag{5}$$

with $D_{C_i} = D_{\mathrm{bio}}$ for $z \leq z_{\mathrm{bio}}$ and $D_{C_i} = 0$ for $z > z_{\mathrm{bio}}$. Integration of equations (5) yields the following general solutions:

I. Bioturbated layer ($z \leq z_{bio}$)

$$\begin{aligned} C_i^I(z) &= A_{1i} \cdot exp(a_{1i}z) + B_{1i} \cdot exp(b_{1i}z) \\ &\overset{\mathrm{BC1)}}{=} A_{1i} \cdot [exp(a_{1i}z) - exp(b_{1i}z)] + C_{0i} \cdot exp(b_{1i}z) \end{aligned} \tag{6}$$

II. Non-bioturbated layer ($z_{bio} < z < z_{ox}$)

$$C_i^{II}(z) = A_{2i} \cdot exp(a_{2i}z) \tag{7}$$

where

$$a_{1i} = \frac{w - \sqrt{w^2 + 4D_{C_i} \cdot k_i}}{2D_{C_i}}, \quad b_{1i} = \frac{w + \sqrt{w^2 + 4D_{C_i} \cdot k_i}}{2D_{C_i}}, \quad a_{2i} = -\frac{k_i}{w} \tag{8}$$

Determining the integration constants ($A_{1,i},\ B_{1,i},\ A_{2,i}$) requires the definition of a set of boundary conditions (Table 2). For organic matter, OMEN-SED applies a known concentration/flux at the sediment-water interface and assumes continuity across the bottom of the bioturbated zone, z_{bio}. See Section 2.3.1 for further details on how to find the analytical solution.

2.2.2 Oxygen

OMEN-SED explicitly accounts for oxygen consumption by the aerobic degradation of organic matter within the oxic zone, as well as the oxidation of reduced species (e.g. NH_4, H_2S, CH_4) produced in the anoxic layers of the sediment (here all zones $z < z_{\mathrm{ox}}$ combined). In the oxic layer ($z < z_{ox}$), the aerobic degradation consumes oxygen with a fixed $O_2 : C$ ratio (O_2C, Tab. 10). A predefined

Table 2. OM Boundary conditions applied in OMEN-SED. For the boundaries we define: $z^-_{\mathrm{bio}} := \lim_{h\to 0}(z_{\mathrm{bio}} - h)$ and $z^+_{\mathrm{bio}} := \lim_{h\to 0}(z_{\mathrm{bio}} + h)$. **Awesome! Du bist ja doch ein Mathematiker!**

DH: A very poor one though ;)

Boundary	**Condition**	
$z = 0$	known concentration	1) $C_i(0) = C_{0i}$
$z = z_{\mathrm{bio}}$	continuity	2) $C_i(z^-_{\mathrm{bio}})$=$C_i(z^+_{\mathrm{bio}})$
		3) $-D_{\mathrm{bio}} \cdot \frac{\partial C_i}{\partial z}\vert_{z^-_{\mathrm{bio}}} = 0$

fraction, $\gamma_{\mathrm{NH_4}}$, of the ammonium produced during the aerobic degradation of OM is nitrified to nitrate, consuming two moles of oxygen per mole of ammonium produced. In addition, OMEN-SED implicitly accounts for the oxygen consumption due to oxidation of reduced species ($\mathrm{NH_4}$, $\mathrm{H_2S}$) produced below the oxic layer through the flux boundary condition at the dynamically calculated (**SA:** see section ?? for details) oxygen penetration depth z_{ox}. This simplification can be justified as it has been shown that these secondary redox reactions mainly occur at the oxic/anoxic interface (Soetaert et al., 1996b). All oxygen consumption processes can thus be formulated as a function of organic matter degradation. The conservation equation for oxygen is given by: **SA: I'd show the POC substitution in the equations below**:

DH: comment Sandra, which Section do you mean here?

DH: you mean the way I did it or in the solution? I think it's easier to understand (also how to get the solution) if it's done in the ODE

$$\frac{\partial \mathrm{O_2}}{\partial t} = 0 = D_{\mathrm{O_2}} \frac{\partial^2 \mathrm{O_2}}{\partial z^2} - w \frac{\partial \mathrm{O_2}}{\partial z} - \frac{1-\phi}{\phi} \sum_i k_i \cdot [\mathrm{O_2C} + 2\gamma_{\mathrm{NH_4}} \mathrm{NC_i}] \cdot C_i(z) \tag{9}$$

I Bioturbated layer ($z \leq z_{\mathrm{bio}}$)

$$\frac{\partial \mathrm{O_2^I}}{\partial t} \overset{6}{=} D^I_{\mathrm{O_2}} \frac{\partial^2 \mathrm{O_2}}{\partial z^2} - w \frac{\partial \mathrm{O_2}}{\partial z} - \frac{1-\phi}{\phi} \sum_i k_i \cdot [\mathrm{O_2C} + 2\gamma_{\mathrm{NH_4}} \mathrm{NC_i}] \cdot \Big(A_{1i} \cdot [exp(a_{1i} z) - exp(b_{1i} z)] + C_{0i} \cdot exp(b_{1i} z) \Big)$$

II Non-bioturbated layer ($z_{\mathrm{bio}} < z < z_{\mathrm{ox}}$)

$$\frac{\partial {\mathrm{O_2}}^{II}}{\partial t} \overset{7}{=} D^{II}_{\mathrm{O_2}} \frac{\partial^2 \mathrm{O_2}}{\partial z^2} - w \frac{\partial \mathrm{O_2}}{\partial z} - \frac{1-\phi}{\phi} \sum_i k_i \cdot [\mathrm{O_2C} + 2\gamma_{\mathrm{NH_4}} \mathrm{NC_i}] \cdot \Big(A_{2i} \cdot exp(a_{2i} z) \Big)$$

where $D^I_{\mathrm{O_2}}$ and $D^{II}_{\mathrm{O_2}}$ denote the $\mathrm{O_2}$ diffusion coefficient for the bioturbated and non-bioturbated layer, respectively. The term $\frac{1-\phi}{\phi}$ accounts for the volume conversion from solid to dissolved phase and $\mathrm{NC_i}$ is the nitrogen to carbon ratio in OM. **SA: explain all terms**

DH: Other terms are explained earlier in 2.2.2 or 2.2.1

Integration yields the following analytical solution for each layer:

I Bioturbated layer ($z \leq z_{\mathrm{bio}}$):

$${\mathrm{O_2}}^I(z) = A^1_{\mathrm{O_2}} + B^1_{\mathrm{O_2}} \cdot \exp(b^1_{\mathrm{O_2}} z) + \sum_i \Phi^I_{1,i} \cdot \exp(a_{1i} z) + \sum_i \Phi^{II}_{1,i} \cdot \exp(b_{1i} z) + \sum_i \Phi^{III}_{1,i} \cdot \exp(b_{1i} z) \tag{10}$$

Table 3. Boundary conditions for oxygen. For the boundaries we define: $z_{\mathrm{bio}}^{-} := \lim_{h\to 0}(z_{\mathrm{bio}} - h)$ and $z_{\mathrm{bio}}^{+} := \lim_{h\to 0}(z_{\mathrm{bio}} + h)$.

Boundary	**Condition**	
$z = 0$	known concentration	1) $\mathrm{O_2}(0) = O_{20}$
$z = z_{\mathrm{bio}}$	continuity	2) $\mathrm{O_2}(z_{\mathrm{bio}}^{-})$=$\mathrm{O_2}(z_{\mathrm{bio}}^{+})$
		3) $-(D_{\mathrm{O_2},0} + D_{\mathrm{bio}}) \cdot \frac{\partial \mathrm{O_2}}{\partial z}\big\vert_{z_{\mathrm{bio}}^{-}} = -D_{\mathrm{O_2},0} \cdot \frac{\partial \mathrm{O_2}}{\partial z}\big\vert_{z_{\mathrm{bio}}^{+}}$
$z = z_{\mathrm{ox}}$	$\mathrm{O_2}$ consumption	4) **IF** $(\mathrm{O_2}(z_\infty) > 0)$
	($z_{\mathrm{ox}} = z_\infty$)	$\frac{\partial \mathrm{O_2}}{\partial z}\vert_{z_{\mathrm{ox}}} = 0$
		ELSE
	($z_{\mathrm{ox}} < z_\infty$)	$\mathrm{O_2}(z_{\mathrm{ox}}) = 0$ and $-D_{\mathrm{O_2}} \cdot \frac{\partial \mathrm{O_2}}{\partial z}\vert_{z_{\mathrm{ox}}} = F_{red}(z_{\mathrm{ox}})$
	with flux from below	$F_{red}(z_{\mathrm{ox}}) = \frac{1-\phi}{\phi} \cdot \int_{z_{\mathrm{ox}}}^{\infty} \sum_i (2\gamma_{\mathrm{NH_4}}\mathrm{NC_i} + 2\gamma_{\mathrm{H_2S}}\mathrm{SO_4C})\, k_i C_i \, dz$

II Non-bioturbated layer ($z_{\mathrm{bio}} < z < z_{\mathrm{ox}}$)

$$\mathrm{O_2}^{II}(z) = A^2_{\mathrm{O_2}} + B^2_{\mathrm{O_2}} \cdot \exp(b^2_{\mathrm{O_2}} z) + \sum_i \Phi^I_{i,2} \cdot \exp(a_{2i} z) \tag{11}$$

with

$$b^1_{\mathrm{O_2}} = \frac{w}{D^I_{\mathrm{O_2}}}, \quad b^2_{\mathrm{O_2}} = \frac{w}{D^{II}_{\mathrm{O_2}}}$$

$$\Phi^I_{1,i} = \frac{1-\phi}{\phi} \cdot \frac{k_i \cdot (\mathrm{O_2C} + 2\gamma_{\mathrm{NH_4}}\mathrm{NC_i}) \cdot A_{1i}}{D^I_{\mathrm{O_2}}(-a_{1i})^2 - w \cdot (-a_{1i})}, \qquad \Phi^{II}_{1,i} = -\frac{1-\phi}{\phi} \cdot \frac{k_i \cdot (\mathrm{O_2C} + 2\gamma_{\mathrm{NH_4}}\mathrm{NC_i}) \cdot A_{1i}}{D^I_{\mathrm{O_2}}(-b_{1i})^2 - w \cdot (-b_{1i})}$$

$$\Phi^{III}_{1,i} = \frac{1-\phi}{\phi} \cdot \frac{k_i \cdot (\mathrm{O_2C} + 2\gamma_{\mathrm{NH_4}}\mathrm{NC_i}) \cdot C_{0i}}{D^I_{\mathrm{O_2}}(-b_{1i})^2 - w \cdot (-b_{1i})}$$

$$\Phi^I_{i,2} := \frac{1-\phi}{\phi} \cdot \frac{k_i \cdot (\mathrm{O_2C} + 2\gamma_{\mathrm{NH_4}}\mathrm{NC_i}) \cdot A_{2i}}{D^{II}_{\mathrm{O_2}}(-a_{2i})^2 - w \cdot (-a_{2i})}$$

Determining the four integration constants ($A^1_{\mathrm{O_2}}$, $B^1_{\mathrm{O_2}}$, $A^2_{\mathrm{O_2}}$, $B^2_{\mathrm{O_2}}$), as well as the $a-priori$ unknown oxygen penetration depth requires the definition of five boundary conditions (see Table 3). At the sediment-water interface, OMEN-SED applies a Dirichlet condition (i.e. known concentration) and assumes concentration and flux continuity across the bottom of the bioturbated zone, z_{bio}. The oxygen penetration depth z_{ox} marks the lower boundary and is dynamically calculated as the depth at which $\mathrm{O_2}(z) = 0$ (see Section 2.3.1). Therefore, OMEN-SED applies a Dirichlet boundary condition $\mathrm{O_2}(z_{\mathrm{ox}}) = 0$ at z_{ox}. In addition, a flux boundary is applied that implicitly accounts for the oxygen consumption by the partial oxidation of $\mathrm{NH_4}$ and $\mathrm{H_2S}$ diffusing into the oxic layer from below. It is assumed that respective fractions ($\gamma_{\mathrm{NH_4}}$ and $\gamma_{\mathrm{H_2S}}$) are directly re-oxidised at the oxic/anoxic interface. Alternatively if $z_{\mathrm{ox}} = z_\infty$, a zero flux boundary condition is applied as lower boundary condition.

2.2.3 Nitrate and Ammonium

Nitrogen dynamics in OMEN-SED are controlled by the metabolic production of ammonium, nitrification, denitrification as well as ammonium adsorption. Ammonium is produced by organic matter degradation in both the oxic and anoxic zones, while denitrification consumes nitrate in the denitrification layer with a fixed $NO_3 : C$ ratio (NO_3C, Tab. 10) **SA: need explanation**. The adsorption of ammonium to sediment particles is formulated as an equilibrium process with constant equilibrium adsorption coefficient K_{NH_4}, thus assuming that the adsorption is fast compared with the characteristic time scales of transport processes (Wang and Van Cappellen, 1996). In addition, a defined fraction, γ_{NH_4}, of metabolically produced ammonium is directly nitrified to nitrate in the oxic zone, while the nitrification of upward diffusing ammonium produced in the sulfidic and methanic layers is implicitly accounted for in the boundary conditions. The conservation equations for ammonium and nitrate are thus given by:

DH: explanation sufficient?

1. Oxic layer ($z \leq z_{ox}$)

$$\frac{\partial {NO_3}^I}{\partial t} = 0 = D_{NO_3} \frac{\partial^2 {NO_3}^I}{\partial z^2} - w \frac{\partial {NO_3}^I}{\partial z} + \gamma_{NH_4} \frac{1-\phi}{\phi} \cdot \sum_i NC_i \cdot k_i \cdot C_i(z) \tag{12}$$

$$\frac{\partial {NH_4}^I}{\partial t} = 0 = \frac{D_{NH_4}}{1+K_{NH_4}} \frac{\partial^2 {NH_4}^I}{\partial z^2} - w \frac{\partial {NH_4}^I}{\partial z} + \frac{1-\gamma_{NH_4}}{1+K_{NH_4}} \cdot \frac{1-\phi}{\phi} \cdot \sum_i NC_i \cdot k_i \cdot C_i(z) \tag{13}$$

2. Denitrification (or nitrogenous) layer ($z_{ox} < z \leq z_{NO_3}$)

$$\frac{\partial {NO_3}^{II}}{\partial t} = 0 = D_{NO_3} \frac{\partial^2 {NO_3}^{II}}{\partial z^2} - w \frac{\partial {NO_3}^{II}}{\partial z} - \frac{1-\phi}{\phi} NO_3C \cdot \sum_i k_i \cdot C_i(z) \tag{14}$$

$$\frac{\partial {NH_4}^{II}}{\partial t} = 0 = \frac{D_{NH_4}}{1+K_{NH_4}} \frac{\partial^2 {NH_4}^{II}}{\partial z^2} - w \frac{\partial {NH_4}^{II}}{\partial z} \tag{15}$$

3. Sulfidic and methanic layer ($z_{NO_3} < z \leq z_\infty$)

$$\frac{\partial {NH_4}^{III}}{\partial t} = 0 = \frac{D_{NH_4}}{1+K_{NH_4}} \frac{\partial^2 {NH_4}^{III}}{\partial z^2} - w \frac{\partial {NH_4}^{III}}{\partial z} + \frac{1}{1+K_{NH_4}} \cdot \frac{1-\phi}{\phi} \cdot \sum_i NC_i \cdot k_i \cdot C_i(z) \tag{16}$$

where D_{NO_3} and D_{NH_4} denote the diffusion coefficients for NO_3 and NH_4 which depend on the bioturbation status of the respective geochemical layer (compare Section 2.3.1). **explain all things and also point out that D dependent on where the redox boundaries are located with respect to zbio** Integration of Eq. (12) - (16) yields the analytical solutions, which are not further developed here but follow the procedure outlined in Section 2.2.2 for oxygen (also see Section 2.3.1 for more details on how to find the analytical solution). Table 4 summarises the boundary conditions applied in OMEN-SED to solve Eq. (12) - (16). The model assumes known bottom water concentrations

DH: all other params explained earlier

Table 4. Boundary conditions for nitrate and ammonium. For the boundaries we define: $z_{\_}^{-} := \lim_{h\to 0}(z_{\_} - h)$ and $z_{\_}^{+} := \lim_{h\to 0}(z_{\_} + h)$.

Boundary	**Condition**	
$z = 0$	known concentration	1) $\mathrm{NO_3}(0) = \mathrm{NO_{30}}$
$z = z_{\mathrm{bio}}$	continuity	2) $\mathrm{NO_3}(z_{\mathrm{bio}}^{-})$=$\mathrm{NO_3}(z_{\mathrm{bio}}^{+})$
		3) $-(D_{\mathrm{NO_3},0} + D_{\mathrm{bio}}) \cdot \frac{\partial \mathrm{NO_3}}{\partial z}\big\vert_{z_{\mathrm{bio}}^{-}} = -D_{\mathrm{NO_3},0} \cdot \frac{\partial \mathrm{NO_3}}{\partial z}\big\vert_{z_{\mathrm{bio}}^{+}}$
$z = z_{\mathrm{ox}}$	continuity	4) $\mathrm{NO_3}(z_{\mathrm{ox}}^{-})$=$\mathrm{NO_3}(z_{\mathrm{ox}}^{+})$
		5) $-D_{\mathrm{NO_3}} \cdot \frac{\partial \mathrm{NO_3}}{\partial z}\big\vert_{z_{\mathrm{ox}}^{-}} + \gamma_{\mathrm{NH_4}} \cdot F_{\mathrm{NH_4}}(z_{\mathrm{ox}}) = -D_{\mathrm{NO_3}} \cdot \frac{\partial \mathrm{NO_3}}{\partial z}\big\vert_{z_{\mathrm{ox}}^{+}}$
	where:	$F_{\mathrm{NH_4}}(z_{\mathrm{ox}}) = \frac{1}{1+K_{\mathrm{NH_4}}} \cdot \frac{1-\phi}{\phi} \cdot \int_{z_{\mathrm{NO_3}}}^{\infty} \sum_i k_i \cdot \mathrm{NC_i} \cdot C_i \, dz$
$z = z_{\mathrm{NO_3}}$	$\mathrm{NO_3}$ consumption	6) **IF** $(\mathrm{NO_3}(z_\infty) > 0)$
	$(z_{\mathrm{NO_3}} = z_\infty)$	$\frac{\partial \mathrm{NO_3}}{\partial z}\big\vert_{z_{\mathrm{NO_3}}} = 0$
		ELSE
	$(z_{\mathrm{NO_3}} < z_\infty)$	$\mathrm{NO_3}(z_{\mathrm{NO_3}}) = 0$
$z = 0$	known concentration	1) $\mathrm{NH_4}(0) = \mathrm{NH_{40}}$
$z = z_{\mathrm{bio}}$	continuity	2) $\mathrm{NH_4}(z_{\mathrm{bio}}^{-})$=$\mathrm{NH_4}(z_{\mathrm{bio}}^{+})$
		3) $-\frac{D_{\mathrm{NH_4},0}+D_{\mathrm{bio}}}{1+K_{\mathrm{NH_4}}} \cdot \frac{\partial \mathrm{NH_4}}{\partial z}\big\vert_{z_{\mathrm{bio}}^{-}} = -\frac{D_{\mathrm{NH_4},0}}{1+K_{\mathrm{NH_4}}} \cdot \frac{\partial \mathrm{NH_4}}{\partial z}\big\vert_{z_{\mathrm{bio}}^{+}}$
$z = z_{\mathrm{ox}}$	continuity	4) $\mathrm{NH_4}(z_{\mathrm{ox}}^{-})$=$\mathrm{NH_4}(z_{\mathrm{ox}}^{+})$
		5) $-\frac{D_{\mathrm{NH_4}}}{1+K_{\mathrm{NH_4}}} \cdot \frac{\partial \mathrm{NH_4}}{\partial z}\big\vert_{z_{\mathrm{ox}}^{-}} - \gamma_{\mathrm{NH_4}} \cdot F_{\mathrm{NH_4}}(z_{\mathrm{ox}}) = -\frac{D_{\mathrm{NH_4}}}{1+K_{\mathrm{NH_4}}} \cdot \frac{\partial \mathrm{NH_4}}{\partial z}\big\vert_{z_{\mathrm{ox}}^{+}}$
	where:	$F_{\mathrm{NH_4}}(z_{\mathrm{ox}}) = \frac{1}{1+K_{\mathrm{NH_4}}} \cdot \frac{1-\phi}{\phi} \cdot \int_{z_{\mathrm{NO_3}}}^{\infty} \sum_i k_i \cdot \mathrm{NC_i} \cdot C_i \, dz$
$z = z_{\mathrm{NO_3}}$	continuity	6) $\mathrm{NH_4}(z_{\mathrm{NO_3}}^{-})$=$\mathrm{NH_4}(z_{\mathrm{NO_3}}^{+})$
	flux	7) $-\frac{D_{\mathrm{NH_4}}}{1+K_{\mathrm{NH_4}}} \cdot \frac{\partial \mathrm{NH_4}}{\partial z}\big\vert_{z_{\mathrm{NO_3}}^{-}} = -\frac{D_{\mathrm{NH_4}}}{1+K_{\mathrm{NH_4}}} \cdot \frac{\partial \mathrm{NH_4}}{\partial z}\big\vert_{z_{\mathrm{NO_3}}^{+}}$
$z = z_\infty$	zero $\mathrm{NH_4}$ flux	8) $\frac{\partial \mathrm{NH_4}}{\partial z}\big\vert_{z_\infty} = 0$

for both species, the complete consumption of nitrate at the nitrate penetration depth (or zero flux if $z_{\mathrm{NO_3}} = z_\infty$) and no change in ammonium flux at z_∞. In addition, concentration and diffusive flux continuity across z_{bio} and z_{ox} is considered for $\mathrm{NO_3}$ and $\mathrm{NH_4}$. Furthermore, the re-oxidation of upward-diffusing reduced ammonium is accounted for in the oxic-anoxic boundary condition for nitrate and ammonium.

2.2.4 Sulfate and Sulfide

Below the denitrification layer ($z > z_{\mathrm{NO_3}}$), organic matter degradation is coupled to sulfate reduction, consuming sulfate and producing hydrogen sulfide with a fixed $\mathrm{SO_4} : \mathrm{C}$ ratio ($\mathrm{SO_4C}$, Tab. 10). In addition, the anaerobic oxidation of upward diffusing methane (AOM) produced below the sulfate penetration and the associated consumption of sulfate and production of sulfide; as well as the production of sulfate and consumption of sulfide through sulfide oxidation are implicitly accounted for through the boundary conditions (Table 5). The conservation equations for sulfate and sulfide are thus given by:

1. Oxic and nitrogenous layer ($z \leq z_{\mathrm{NO_3}}$)

$$\frac{\partial \mathrm{SO_4}^I}{\partial t} = 0 = D_{\mathrm{SO_4}} \frac{\partial^2 \mathrm{SO_4}^I}{\partial z^2} - w \frac{\partial \mathrm{SO_4}^I}{\partial z} \tag{17}$$

$$\frac{\partial \mathrm{H_2S}^I}{\partial t} = 0 = D_{\mathrm{H_2S}} \frac{\partial^2 \mathrm{H_2S}^I}{\partial z^2} - w \frac{\partial \mathrm{H_2S}^I}{\partial z} \tag{18}$$

2.Sulfidic layer ($z_{\mathrm{NO_3}} < z \leq z_{\mathrm{SO_4}}$)

$$\frac{\partial \mathrm{SO_4}^{II}}{\partial t} = 0 = D_{\mathrm{SO_4}} \frac{\partial^2 \mathrm{SO_4}^{II}}{\partial z^2} - w \frac{\partial \mathrm{SO_4}^{II}}{\partial z} - \frac{1-\phi}{\phi} \cdot \sum_i \mathrm{SO_4C} \cdot k_i \cdot C_i(z) \tag{19}$$

$$\frac{\partial \mathrm{H_2S}^{II}}{\partial t} = 0 = D_{\mathrm{H_2S}} \frac{\partial^2 \mathrm{H_2S}^{II}}{\partial z^2} - w \frac{\partial \mathrm{H_2S}^{II}}{\partial z} + \frac{1-\phi}{\phi} \cdot \sum_i \mathrm{SO_4C} \cdot k_i \cdot C_i(z) \tag{20}$$

3. Methanic layer ($z_{\mathrm{SO_4}} < z \leq z_\infty$)

$$\frac{\partial \mathrm{H_2S}^{III}}{\partial t} = 0 = D_{\mathrm{H_2S}} \frac{\partial^2 \mathrm{H_2S}^{III}}{\partial z^2} - w \frac{\partial \mathrm{H_2S}^{III}}{\partial z} \tag{21}$$

where $D_{\mathrm{SO_4}}$ and $D_{\mathrm{H_2S}}$ denote the diffusion coefficients for $\mathrm{SO_4}$ and $\mathrm{H_4S}$ which depend on the bioturbation status of the respective geochemical layer (compare Section 2.3.1). Integration of Eq. (17) - (21) yields the analytical solution and Table 5 summarises the boundary conditions applied. OMEN-SED assumes known concentrations at the sediment-water interface and continuity across the bioturbation depth and the nitrate penetration depth. The re-oxidation of reduced $\mathrm{H_2S}$ to $\mathrm{SO_4}$ is accounted for implicitly via the oxic-anoxic boundary condition for both species, while reduction of $\mathrm{SO_4}$ and the associated production of $\mathrm{H_2S}$ via AOM is accounted for through the respective boundary conditions at $z_{\mathrm{SO_4}}$. In case $z_{\mathrm{SO_4}} < z_\infty$, OMEN-SED assumes zero sulfate concentration at $z_{\mathrm{SO_4}}$ and its diffusive flux must equal the amount of methane produced below; or, in case $z_{\mathrm{SO_4}} = z_\infty$, a zero flux condition for sulfate is considered. At the lower boundary z_∞ zero flux of $\mathrm{H_2S}$ is considered.

2.2.5 Phosphate

The biogeochemical description of phosphorus (P) dynamics builds on the work of Slomp et al. (1996) and accounts for phosphorous recycling through organic matter degradation, adsorption onto sediments and iron-hydroxides, as well as apatite formation (see Figure 2 for a schematic overview of the sedimentary P cycle). In the oxic zone of the sediment, $\mathrm{PO_4}$ liberated through organic matter degradation can adsorb to iron-hydroxides forming Fe-bound P (or M, Slomp et al., 1998). Below the oxic zone, $\mathrm{PO_4}$ is not only produced via organic matter degradation but can also be released from the Fe-bound P pool due to the reduction of Fe oxides under anoxic conditions. Furthermore, in these zones phosphate concentrations build up and pore waters can thus become over-saturated

Table 5. Boundary conditions for sulfate and sulfide. For the boundaries we define: $z_{\_}^{-} := \lim_{h\to 0}(z_{\_} - h)$ and $z_{\_}^{+} := \lim_{h\to 0}(z_{\_} + h)$.

Boundary	**Condition**		
$z = 0$	known concentration	1)	$SO_4(0)$=SO_{40}
$z = z_{\mathrm{bio}}$	continuity	2)	$SO_4(z_{\mathrm{bio}}^{-})$=$SO_4(z_{\mathrm{bio}}^{+})$
	flux	3)	$-(D_{SO_4,0} + D_{\mathrm{bio}}) \cdot \frac{\partial SO_4}{\partial z}\vert_{z_{\mathrm{bio}}^{-}} = -D_{SO_4,0} \cdot \frac{\partial SO_4}{\partial z}\vert_{z_{\mathrm{bio}}^{+}}$
$z = z_{\mathrm{ox}}$	continuity	4)	$SO_4(z_{\mathrm{ox}}^{-})$=$SO_4(z_{\mathrm{ox}}^{+})$
	flux	5)	$-D_{SO_4} \cdot \frac{\partial SO_4}{\partial z}\vert_{z_{\mathrm{ox}}^{-}} + \gamma_{H_2S} \cdot F_{H_2S}(z_{\mathrm{ox}}) = -D_{SO_4} \cdot \frac{\partial SO_4}{\partial z}\vert_{z_{\mathrm{ox}}^{+}}$
	where:		$F_{H_2S}(z_{\mathrm{ox}}) = \frac{1-\phi}{\phi} \cdot \left(\int_{z_{NO_3}}^{SO_4} \sum_i SO_4C \cdot k_i \cdot C_i \, dz + \gamma_{CH_4} \cdot \int_{z_{SO_4}}^{\infty} \sum_i MC \cdot k_i \cdot C_i \, dz \right)$
$z = z_{NO_3}$	continuity	6)	$SO_4(z_{NO_3}^{-})$=$SO_4(z_{NO_3}^{+})$
	flux	7)	$-D_{SO_4} \cdot \frac{\partial SO_4}{\partial z}\vert_{z_{NO_3}^{-}} = -D_{SO_4} \cdot \frac{\partial SO_4}{\partial z}\vert_{z_{NO_3}^{+}}$
$z = z_{SO_4}$	SO_4 consumption	8)	**IF** $(SO_4(z_\infty) > 0)$
	$(z_{SO_4} = z_\infty)$		$\frac{\partial SO_4}{\partial z}\vert_{z_{SO_4}} = 0$
			ELSE
	$(z_{SO_4} < z_\infty)$		$SO_4(z_{SO_4}) = 0$ and $-D_{SO_4} \cdot \frac{\partial SO_4}{\partial z}\vert_{z_{SO_4}} = \gamma_{CH_4} \cdot F_{CH_4}(z_{SO_4})$
	with flux from below:		$F_{CH_4}(z_{SO_4}) = \frac{1-\phi}{\phi} \cdot \int_{z_{SO_4}}^{\infty} \sum_i MC \cdot k_i \cdot C_i \, dz$
$z = 0$	known concentration	1)	$H_2S(0) = H_2S_0$
$z = z_{\mathrm{bio}}$	continuity	2)	$H_2S(z_{\mathrm{bio}}^{-})$=$H_2S(z_{\mathrm{bio}}^{+})$
	flux	3)	$-(D_{H_2S,0} + D_{\mathrm{bio}}) \cdot \frac{\partial H_2S}{\partial z}\vert_{z_{\mathrm{bio}}^{-}} = -D_{H_2S,0} \cdot \frac{\partial H_2S}{\partial z}\vert_{z_{\mathrm{bio}}^{+}}$
$z = z_{\mathrm{ox}}$	continuity	4)	$H_2S(z_{\mathrm{ox}}^{-})$=$H_2S(z_{\mathrm{ox}}^{+})$
	flux	5)	$-D_{H_2S} \cdot \frac{\partial H_2S}{\partial z}\vert_{z_{\mathrm{ox}}^{-}} - \gamma_{H_2S} F_{H_2S}(z_{\mathrm{ox}}) = -D_{H_2S} \cdot \frac{\partial H_2S}{\partial z}\vert_{z_{\mathrm{ox}}^{+}}$
	where:		$F_{H_2S}(z_{\mathrm{ox}}) = \frac{1-\phi}{\phi} \cdot \left(\int_{z_{NO_3}}^{SO_4} \sum_i SO_4C \cdot k_i \cdot C_i \, dz + \gamma_{CH_4} \cdot \int_{z_{SO_4}}^{\infty} \sum_i MC \cdot k_i \cdot C_i \, dz \right)$
$z = z_{NO_3}$	continuity	6)	$H_2S(z_{NO_3}^{-})$=$H_2S(z_{NO_3}^{+})$
	flux	7)	$-D_{H_2S} \cdot \frac{\partial H_2S}{\partial z}\vert_{z_{NO_3}^{-}} = -D_{H_2S} \cdot \frac{\partial H_2S}{\partial z}\vert_{z_{NO_3}^{+}}$
$z = z_{SO_4}$	continuity	8)	$H_2S(z_{SO_4}^{-})$=$H_2S(z_{SO_4}^{+})$
	flux (with AOM)	9)	$-D_{H_2S} \cdot \frac{\partial H_2S}{\partial z}\vert_{z_{SO_4}^{-}} + \gamma_{CH_4} \cdot F_{CH_4}(z_{SO_4}) = -D_{H_2S} \cdot \frac{\partial H_2S}{\partial z}\vert_{z_{SO_4}^{+}}$
	where:		$F_{CH_4}(z_{SO_4}) = \frac{1-\phi}{\phi} \cdot \int_{z_{SO_4}}^{\infty} \sum_i MC \cdot k_i \cdot C_i \, dz$
$z = z_\infty$	zero H_2S flux	10)	$\frac{\partial H_2S}{\partial z}\vert_{z_\infty} = 0$

DH: @Sandra: BC 5) Include $\int_{z_{SO_4}}^{\infty}$ here?

DH: @Sandra: think yes, because at 8) CH_4 from $\int_{z_{SO_4}}^{\infty}$ is oxidised to H_2S; at 5) this H_2S to SO_4

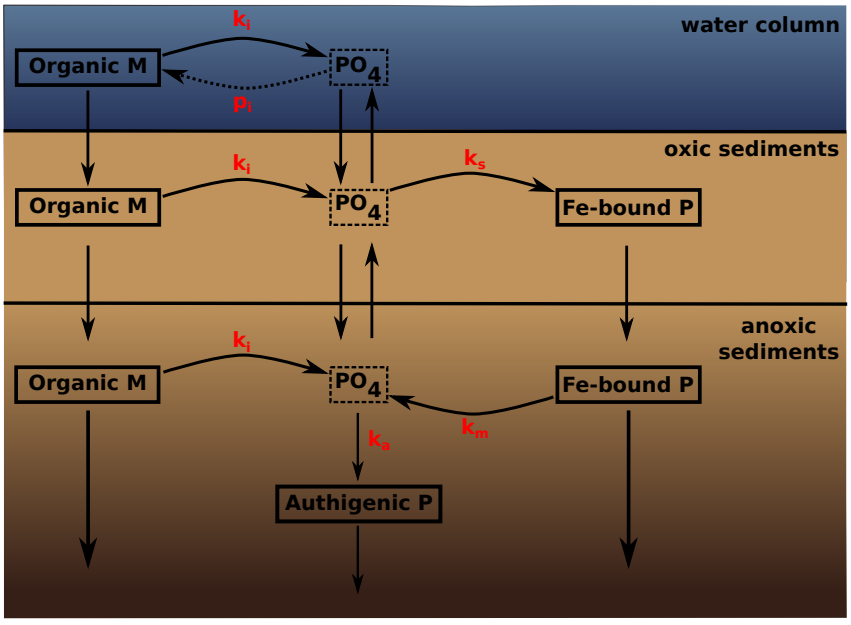

Figure 2. A schematic of the sedimentary P cycle in OMEN-SED. Red numbers represent kinetic rate constants for phosphorus dynamics (compare Table 10; p_i represents uptake rate of PO_4 via primary production in shallow environments). Adapted from Slomp et al. (1996).

with respect to apatite, thus triggering the authigenic formation of apatite (Van Cappellen and Berner, 1988). Phosphorus bound in authigenic minerals represents a permanent sink for reactive phosphorus (Slomp et al., 1996). As for ammonium, the adsorption of P to the sediment matrix is treated as an equilibrium processes, parameterised with dimensionless adsorption coefficients for the oxic and anoxic zone, respectively ($K^{\mathrm{ox}}_{\mathrm{PO_4}}$, $K^{\mathrm{anox}}_{\mathrm{PO_4}}$ Slomp et al., 1998). The sorption and desorption of P to iron-hydroxides as well as the authigenic apatite formation are described as first-order reactions with rate constants k_s, k_m and k_a, respectively (Table 10). The rate of the respective process is calculated as the product of the rate constant and the difference between the current concentration (of $\mathrm{PO_4}$ and M) and an equilibrium or asymptotic concentration Slomp et al. (1996). The asymptotic Fe-bound P concentration is M^{∞} and the equilibrium concentration for P sorption and authigenic apatite formation are ${\mathrm{PO_4}}^s$ and ${\mathrm{PO_4}}^a$, respectively (Table 10).

DH: enough Info on Fe-adsorption and M?

1. Oxic layer ($z \leq z_{\mathrm{ox}}$)

$$\frac{\partial {\mathrm{PO_4}}^I}{\partial t} = \frac{D_{\mathrm{PO_4}}}{1+K^{\mathrm{ox}}_{\mathrm{PO_4}}}\frac{\partial^2 {\mathrm{PO_4}}^I}{\partial z^2} - w\frac{\partial {\mathrm{PO_4}}^I}{\partial z} + \frac{1-\phi}{\phi}\frac{1}{1+K^{\mathrm{ox}}_{\mathrm{PO_4}}}\sum_i (\mathrm{PC}_i \cdot k_i \cdot C_i(z)) - \frac{k_s}{1+K^{\mathrm{ox}}_{\mathrm{PO_4}}}({\mathrm{PO_4}}^I - {\mathrm{PO_4}}^s) \quad (22)$$

$$\frac{\partial \mathrm{M}^I}{\partial t} = D_{\mathrm{M}}\frac{\partial^2 \mathrm{M}^I}{\partial z^2} - w\frac{\partial \mathrm{M}^I}{\partial z} + \frac{\phi}{1-\phi}k_s({\mathrm{PO_4}}^I - {\mathrm{PO_4}}^s) \quad (23)$$

Table 6. Boundary conditions for phosphate and Fe-bound P (M). For the boundaries we define: $z_{\_}^{-} := \lim_{h\to 0}(z_{\_} - h)$ and $z_{\_}^{+} := \lim_{h\to 0}(z_{\_} + h)$.

Boundary	**Condition**	
$z = 0$	known concentration	1) $\mathrm{PO_4}(0)$=$\mathrm{PO_{40}}$
$z = z_{\mathrm{bio}}$	continuity	2) $\mathrm{PO_4}(z_{\mathrm{bio}}^{-})$=$\mathrm{PO_4}(z_{\mathrm{bio}}^{+})$
	flux	3) $(D_{\mathrm{PO_4},0} + D_{\mathrm{bio}}) \cdot \frac{\partial \mathrm{PO_4}}{\partial z}\vert_{z_{\mathrm{bio}}^{-}} = D_{\mathrm{PO_4},0} \cdot \frac{\partial \mathrm{PO_4}}{\partial z}\vert_{z_{\mathrm{bio}}^{+}}$
$z = z_{\mathrm{ox}}$	continuity	4) $\mathrm{PO_4}(z_{\mathrm{ox}}^{-})$=$\mathrm{PO_4}(z_{\mathrm{ox}}^{+})$
	flux	5) $-\frac{D_{\mathrm{PO_4}}}{1+K_{\mathrm{PO_4}}^{ox}} \cdot \frac{\partial \mathrm{PO_4}}{\partial z}\vert_{z_{\mathrm{ox}}^{-}} = -\frac{D_{\mathrm{PO_4}}}{1+K_{\mathrm{PO_4}}^{\mathrm{anox}}} \cdot \frac{\partial \mathrm{PO_4}}{\partial z}\vert_{z_{\mathrm{ox}}^{+}}$
$z = z_{\infty}$	flux	10) $\frac{\partial \mathrm{PO_4}}{\partial z}\vert_{z_{\infty}} = 0$
$z = 0$	known concentration	1) $\mathrm{M}(0) = \mathrm{M}_0$
$z = z_{\mathrm{bio}}$	continuity	2) $\mathrm{M}(z_{\mathrm{bio}}^{-})$=$\mathrm{M}(z_{\mathrm{bio}}^{+})$
	flux	3) $\frac{\partial \mathrm{M}}{\partial z}\vert_{z_{\mathrm{bio}}^{-}} = \frac{\partial \mathrm{M}}{\partial z}\vert_{z_{\mathrm{bio}}^{+}}$
$z = z_{\mathrm{ox}}$	continuity	4) $\mathrm{M}(z_{\mathrm{ox}}^{-})$=$\mathrm{M}(z_{\mathrm{ox}}^{+})$
	flux	5) $\frac{\partial \mathrm{M}}{\partial z}\vert_{z_{\mathrm{ox}}^{-}} = \frac{\partial \mathrm{M}}{\partial z}\vert_{z_{\mathrm{ox}}^{+}}$
$z = z_{\infty}$	asymptotic concentration	10) $\mathrm{M}(z_{\infty}) = \mathrm{M}_{\infty}$

2. Anoxic layers ($z_{\mathrm{ox}} < z \leq z_{\infty}$)

$$\frac{\partial \mathrm{M}^{II}}{\partial t} = D_{\mathrm{M}} \frac{\partial^2 \mathrm{M}^{II}}{\partial z^2} - w \frac{\partial \mathrm{M}^{II}}{\partial z} - k_m(\mathrm{M}^{II} - \mathrm{M}^{\infty}) \tag{24}$$

$$\frac{\partial {\mathrm{PO_4}}^{II}}{\partial t} = \frac{D_{\mathrm{PO_4}}}{1+K_{\mathrm{PO_4}}^{\mathrm{anox}}} \frac{\partial^2 {\mathrm{PO_4}}^{II}}{\partial z^2} - w \frac{\partial {\mathrm{PO_4}}^{II}}{\partial z} + \frac{1-\phi}{\phi} \frac{1}{1+K_{\mathrm{PO_4}}^{\mathrm{anox}}} \sum_i (\mathrm{PC}_i \cdot k_i \cdot C_i(z)) - \frac{k_a}{1+K_{\mathrm{PO_4}}^{\mathrm{anox}}} ({\mathrm{PO_4}}^{II} - {\mathrm{PO_4}}^{a}) + \frac{(1-\phi)}{\phi} \frac{k_m}{1+K_{\mathrm{PO_4}}^{\mathrm{anox}}} (\mathrm{M}^{II} - \mathrm{M}^{\infty}) \tag{25}$$

where $D_{\mathrm{PO_4}}$ denotes the diffusion coefficient for $\mathrm{PO_4}$ which depends on the bioturbation status of the respective geochemical layer and $D_{\mathrm{M}} = D_{\mathrm{bio}}$ for $z \leq z_{\mathrm{bio}}$ and $D_{\mathrm{M}} = 0$ for $z > z_{\mathrm{bio}}$ (compare Section 2.3.1). Integration of Eq. (22) - (25) yields the analytical solution and Table 6 summarises the boundary conditions applied in OMEN-SED. The model assumes known bottom water concentrations and equal concentrations and diffusive fluxes at z_{bio} and z_{ox} for both species. A no flux boundary condition is applied at z_{∞}.

DH: I think what I wrote before also applies: a asymptotic Fe-bound P concentration at z_{ox} is assumed!

2.2.6 Dissolved Inorganic Carbon (DIC)

OMEN-SED accounts for the production of dissolved inorganic carbon (DIC) through organic matter degradation, as well as methane oxidation **TODO: need to say something about carbonates here**. Organic matter degradation produces dissolved inorganic carbon with a stoichiometric DIC : C ratio of 1:2 in the methanic zone and 1:1 in the rest of the sediment column ($\mathrm{DICC^{II}}$ and $\mathrm{DICC^{I}}$ respectively). DIC production through methane oxidation is implicitly taken into account through the boundary condition at $z_{\mathrm{SO_4}}$. The conservation equations for DIC are thus given by:

Table 7. Boundary conditions for DIC. For the boundaries we define: $z_{\_}^{-} := \lim_{h\to 0}(z_{\_} - h)$ and $z_{\_}^{+} := \lim_{h\to 0}(z_{\_} + h)$.

Boundary	Condition	
$z = 0$	known concentration	1) $\mathrm{DIC}(0) = \mathrm{DIC}_0$
$z = z_{\mathrm{bio}}$	continuity	2) $\mathrm{DIC}(z_{\mathrm{bio}}^{-})$=$\mathrm{DIC}(z_{\mathrm{bio}}^{+})$
	flux	3) $-(D_{\mathrm{DIC},0} + D_{\mathrm{bio}}) \cdot \frac{\partial \mathrm{DIC}}{\partial z}\vert_{z_{\mathrm{bio}}^{-}} = -D_{\mathrm{DIC},0} \cdot \frac{\partial \mathrm{DIC}}{\partial z}\vert_{z_{\mathrm{bio}}^{+}}$
$z = z_{\mathrm{SO_4}}$	continuity	4) $\mathrm{DIC}(z_{\mathrm{SO_4}}^{-})$=$\mathrm{DIC}(z_{\mathrm{SO_4}}^{+})$
	flux (with AOM)	5) $-D_{\mathrm{DIC}} \cdot \frac{\partial \mathrm{DIC}}{\partial z}\vert_{z_{\mathrm{SO_4}}^{-}} + \gamma_{\mathrm{CH_4}} \cdot F_{\mathrm{CH_4}}(z_{\mathrm{SO_4}}) = -D_{\mathrm{DIC}} \cdot \frac{\partial \mathrm{DIC}}{\partial z}\vert_{z_{\mathrm{SO_4}}^{+}}$
	where:	$F_{\mathrm{CH_4}}(z_{\mathrm{SO_4}}) = \frac{1-\phi}{\phi} \cdot \int_{z_{\mathrm{SO_4}}}^{\infty} \sum_i \mathrm{MC} \cdot k_i \cdot C_i \, dz$
$z = z_{\infty}$	zero DIC flux	6) $\frac{\partial \mathrm{DIC}}{\partial z}\vert_{z_{\infty}} = 0$

1. Oxic, nitrogenous and sulfidic layer ($z \leq z_{\mathrm{SO_4}}$)

$$\frac{\partial \mathrm{DIC}^{I}}{\partial t} = 0 = D_{\mathrm{DIC}} \frac{\partial^2 \mathrm{DIC}^{I}}{\partial z^2} - w \frac{\partial \mathrm{DIC}^{I}}{\partial z} + \frac{1-\phi}{\phi} \cdot \sum_i \mathrm{DICC^{I}} \cdot k_i \cdot C_i(z) \tag{26}$$

2. Methanic layer ($z_{\mathrm{SO_4}} < z \leq z_{\infty}$)

$$\frac{\partial \mathrm{DIC}^{II}}{\partial t} = 0 = D_{\mathrm{DIC}} \frac{\partial^2 \mathrm{DIC}^{II}}{\partial z^2} - w \frac{\partial \mathrm{DIC}^{II}}{\partial z} + \frac{1-\phi}{\phi} \cdot \sum_i \mathrm{DICC^{II}} \cdot k_i \cdot C_i(z) \tag{27}$$

where D_{DIC} denotes the diffusion coefficient for DIC which depends on the bioturbation status of the respective geochemical layer. Integration of Eq. (26) and (27) yields the analytical solution and Table 7 summarises the boundary conditions applied in OMEN-SED. A Dirichlet condition is applied at the sediment-water interface. In addition, the model assumes a zero flux through the lower boundary z_{∞} and continuity across the bottom of the bioturbated zone, as well as the sulfate penetration depth. An additional flux boundary condition at $z_{\mathrm{SO_4}}$, implicitly accounts for DIC production through anaerobic oxidation of methane (Table 7 Eq. 5).

2.2.7 Alkalinity

TODO: again need to mention carboantes Organic matter degradation and secondary redox reactions exert a complex influence on alkalinity (Wolf-Gladrow et al., 2007). To model alkalinity in OMEN-SED the sediment column is partitioned into four geochemical layers, where different equations describe the biogeochemical processes using variable stoichiometric coefficients (compare Tables 10 and 15). Above z_{ox}, the combined effects of $\mathrm{NH_4}$ and P release due to aerobic OM degradation increases alkalinity according to $\mathrm{ALK^{OX}}$ whereas nitrification decreases alkalinity with stoichiometry $\mathrm{ALK^{NIT}}$. In the remaining three zones anaerobic OM degradation generally results in an increase in alkalinity, with the exact magnitude depending on the nature of the terminal electron acceptor used (i.e. $\mathrm{ALK^{DEN}}$, $\mathrm{ALK^{SUL}}$, $\mathrm{ALK^{MET}}$). In addition, the effect of secondary redox

reactions, such as nitrification, methane and sulfide oxidation are implicitly accounted for in the boundary conditions.

In OMEN-SED, the conservation equations for alkalinity is thus given by:

1. Oxic layer ($z \leq z_{\mathrm{ox}}$)

$$\frac{\partial \mathrm{ALK}^{I}}{\partial t} = 0 = D_{\mathrm{ALK}} \frac{\partial^2 \mathrm{ALK}^{I}}{\partial z^2} - w \frac{\partial \mathrm{ALK}^{I}}{\partial z} + \frac{1-\phi}{\phi} \cdot \sum_i \left(\mathrm{ALK}^{\mathrm{NIT}} \cdot \frac{\gamma_{\mathrm{NH_4}}}{1+K_{\mathrm{NH_4}}} \mathrm{NC_i} + \mathrm{ALK}^{\mathrm{OX}} \right) \cdot k_i \cdot C_i(z) \tag{28}$$

2. Dentrification or nitrogenous layer ($z_{\mathrm{ox}} < z \leq z_{\mathrm{NO_3}}$)

$$\frac{\partial \mathrm{ALK}^{II}}{\partial t} = 0 = D_{\mathrm{ALK}} \frac{\partial^2 \mathrm{ALK}^{II}}{\partial z^2} - w \frac{\partial \mathrm{ALK}^{II}}{\partial z} + \frac{1-\phi}{\phi} \cdot \sum_i \mathrm{ALK}^{\mathrm{DEN}} \cdot k_i \cdot C_i(z) \tag{29}$$

3. Sulfidic layer ($z_{\mathrm{NO_3}} < z \leq z_{\mathrm{SO_4}}$)

$$\frac{\partial \mathrm{ALK}^{III}}{\partial t} = 0 = D_{\mathrm{ALK}} \frac{\partial^2 \mathrm{ALK}^{III}}{\partial z^2} - w \frac{\partial \mathrm{ALK}^{III}}{\partial z} + \frac{1-\phi}{\phi} \cdot \sum_i \mathrm{ALK}^{\mathrm{SUL}} \cdot k_i \cdot C_i(z) \tag{30}$$

4. Methanic layer ($z_{\mathrm{SO_4}} < z \leq z_{\infty}$)

$$\frac{\partial \mathrm{ALK}^{IV}}{\partial t} = 0 = D_{\mathrm{ALK}} \frac{\partial^2 \mathrm{ALK}^{IV}}{\partial z^2} - w \frac{\partial \mathrm{ALK}^{IV}}{\partial z} + \frac{1-\phi}{\phi} \cdot \sum_i \mathrm{ALK}^{\mathrm{MET}} \cdot k_i \cdot C_i(z) \tag{31}$$

where D_{ALK} denotes the diffusion coefficient for ALK which depends on the bioturbation status of the respective geochemical layer. Integration of Eq. (28) - (31) yields the analytical solution and Table 8 summarises the boundary conditions applied in OMEN-SED. A Dirichlet boundary condition is applied at the sediment-water interface. The decrease of alkalinity due to oxidation of reduced species produced in the anoxic layers (with stoichiometry $\mathrm{ALK}^{\mathrm{NIT}}$ and $\mathrm{ALK}^{\mathrm{H_2S}}$) is implicitly taken into account through the flux boundary condition at z_{ox} (Table 8 Eq. 5). Furthermore, the oxidation of methane by sulfate reduction increases alkalinity with stoichiometry $\mathrm{ALK}^{\mathrm{AOM}}$ which is accounted for through the flux boundary condition at $z_{\mathrm{SO_4}}$ (Table 8 Eq. 9). At the lower boundary z_{∞} a zero flux condition is applied.

2.3 Determination of Integration Constants

The integration constants of all general analytical solutions derived above change in response to changing boundary conditions. OMEN-SED thus has to re-determine integration constants for each dynamic zone (i.e. $z_{\mathrm{ox}}, z_{\mathrm{bio}}, z_{\mathrm{NO_3}}$ and $z_{\mathrm{SO_4}}$) at every time step. The bioturbation boundary poses a particular challenge as it can theoretically occur in any of the dynamic geochemical zones (compare Fig. 3). Therefore, in order to generalise and simplify this recurring boundary matching problem, an independent algorithm (rather than a fully-worked-out algebraic solution), which only ever has to solve a two-simultaneous-equation problem is implemented.

Table 8. Boundary conditions for alkalinity. For the boundaries we define: $z_{\_}^{-} := \lim_{h\to 0}(z_{\_} - h)$ and $z_{\_}^{+} := \lim_{h\to 0}(z_{\_} + h)$.

Boundary	**Condition**		
$z = 0$	known concentration	1)	$\mathrm{ALK}(0) = \mathrm{ALK}_0$
$z = z_{\mathrm{bio}}$	continuity	2)	$\mathrm{ALK}(z_{\mathrm{bio}}^{-})$=$\mathrm{ALK}(z_{\mathrm{bio}}^{+})$
	flux	3)	$-(D_{\mathrm{ALK},0} + D_{\mathrm{bio}}) \cdot \frac{\partial \mathrm{ALK}}{\partial z}\vert_{z_{\mathrm{bio}}^{-}} = -D_{\mathrm{ALK},0} \cdot \frac{\partial \mathrm{ALK}}{\partial z}\vert_{z_{\mathrm{bio}}^{+}}$
$z = z_{\mathrm{ox}}$	continuity	4)	$\mathrm{ALK}(z_{\mathrm{ox}}^{-})$=$\mathrm{ALK}(z_{\mathrm{ox}}^{+})$
	flux	5)	$-D_{\mathrm{ALK}} \cdot \frac{\partial \mathrm{ALK}}{\partial z}\vert_{z_{\mathrm{ox}}^{-}} + F_{\mathrm{ALK}}(z_{\mathrm{ox}}) = -D_{\mathrm{ALK}} \cdot \frac{\partial \mathrm{ALK}}{\partial z}\vert_{z_{\mathrm{ox}}^{+}}$
	where:		$F_{\mathrm{ALK}}(z_{\mathrm{ox}}) = \frac{1-\phi}{\phi} \cdot \left(\mathrm{ALK}^{\mathrm{H_2S}} \cdot \gamma_{\mathrm{H_2S}} \int_{z_{\mathrm{NO_3}}}^{\mathrm{SO_4}} \sum_i \mathrm{SO_4C} \cdot k_i \cdot C_i \, dz\right)$ $+ \frac{1-\phi}{\phi} \cdot \left(\mathrm{ALK}^{\mathrm{NIT}} \frac{\gamma_{\mathrm{NH_4}}}{1+k_{\mathrm{NH_4}}} \int_{z_{\mathrm{NO_3}}}^{\infty} \sum_i \mathrm{NC_i} \cdot k_i \cdot C_i \, dz\right)$
$z = z_{\mathrm{NO_3}}$	continuity	6)	$\mathrm{ALK}(z_{\mathrm{NO_3}}^{-})$=$\mathrm{ALK}(z_{\mathrm{NO_3}}^{+})$
	flux	7)	$-D_{\mathrm{ALK}} \cdot \frac{\partial \mathrm{ALK}}{\partial z}\vert_{z_{\mathrm{NO_3}}^{-}} = -D_{\mathrm{ALK}} \cdot \frac{\partial \mathrm{ALK}}{\partial z}\vert_{z_{\mathrm{NO_3}}^{+}}$
$z = z_{\mathrm{SO_4}}$	continuity	8)	$\mathrm{ALK}(z_{\mathrm{SO_4}}^{-})$=$\mathrm{ALK}(z_{\mathrm{SO_4}}^{+})$
	flux (with AOM)	9)	$-D_{\mathrm{ALK}} \cdot \frac{\partial \mathrm{ALK}}{\partial z}\vert_{z_{\mathrm{SO_4}}^{-}} + F_{\mathrm{ALK}}(z_{\mathrm{SO_4}}) = -D_{\mathrm{ALK}} \cdot \frac{\partial \mathrm{ALK}}{\partial z}\vert_{z_{\mathrm{SO_4}}^{+}}$
	where:		$F_{\mathrm{ALK}}(z_{\mathrm{SO_4}}) = \frac{1-\phi}{\phi} \cdot \left(\mathrm{ALK}^{\mathrm{AOM}} \gamma_{\mathrm{CH_4}} \cdot \int_{z_{\mathrm{SO_4}}}^{\infty} \sum_i k_i \cdot C_i \, dz\right)$
$z = z_{\infty}$	zero ALK flux	10)	$\frac{\partial \mathrm{ALK}}{\partial z}\vert_{z_{\infty}} = 0$

2.3.1 Generic Boundary Condition Matching (GBCM)

A general steady-state transport-reaction equation for the set of coupled reaction-tansport equations implemented in OMEN-SED can be formulated as:

$$\frac{\partial C}{\partial t} = 0 = D\frac{\partial^2 C}{\partial z^2} - w\frac{\partial C}{\partial z} - \sum_i \alpha_i \exp(-\beta_i z) - k \cdot C + Q. \tag{32}$$

where z is the sediment depth, t the time, D is the diffusion coefficient and w is the advection rate **describe the other parameters too, e.g. alpha, Q etc**.

The solution of Eq. (the above) is of the general form:

$$C(z) = A\exp(az) + B\exp(bz) + \sum_i \frac{\alpha_i}{D\beta_i^2 - w\beta_i - k} \cdot \exp(-\beta_i z) + \frac{Q}{k} \tag{33}$$

and can therefore be expressed as:

$$C(z) = A \cdot E(z) + B \cdot F(z) + G(z) \tag{34}$$

where $E(z)$, $F(z)$ are the homogeneous solutions of the ODE, G(z) the particular integral, and A, B are the integration constants (compare Fig. 3 for the whole sediment column).

Each boundary matching problem involves matching continuity and flux for the two solutions of the respective reaction-transport equation above, $C_U(z)$ (= 'upper'), and below, $C_L(z)$ (= 'lower'), the dynamic boundary at $z = z_b$:

$$C_U(z) = A_U \cdot E_U(z) + B_U \cdot F_U(z) + G_U(z) \tag{35}$$

$$C_L(z) = A_L \cdot E_L(z) + B_L \cdot F_L(z) + G_L(z). \tag{36}$$

OMEN-SED generally applies concentration continuity and flux boundary conditions at its internal, dynamic boundaries:

Continuity (where for generality we allow a discontinuity V_b)

$$C_U(z_b) = C_L(z_b) + V_b \tag{37}$$

Flux

$$D_U C'_U(z_b) + wC_U(z_b) = D_L C'_L(z_b) + wC_L(z_b) + F_b \tag{38}$$

where w is advection, D are the diffusion coefficients and F_b is any flux discontinuity.

Substituting the general ODE solutions (35), (36), the boundary conditions can be thus two equations connecting the four integration constants:

$$\begin{pmatrix} E_U & F_U \\ D_U E'_U & D_U F'_U \end{pmatrix} \begin{pmatrix} A_U \\ B_U \end{pmatrix} = \begin{pmatrix} E_L & F_L \\ D_L E'_L & D_L F'_L \end{pmatrix} \begin{pmatrix} A_L \\ B_L \end{pmatrix} + \begin{pmatrix} G_L - G_U + V_b \\ D_L G'_L - D_U G'_U + F_b - wV_b \end{pmatrix} \tag{39}$$

where the ODE solutions $E,\ F,\ G$ are all evaluated at z_b.

Equation (39) can now be solved to give A_U and B_U as a function of the integration constants from the layer below (A_L and B_L), thereby constructing a piecewise solution for both layers, with just two integration constants (implemented in the function **benthic_utils.matchsoln** of OMEN-SED).

$$\begin{pmatrix} A_U \\ B_U \end{pmatrix} = \begin{pmatrix} c_1 & c_2 \\ c_3 & c_4 \end{pmatrix} \begin{pmatrix} A_L \\ B_L \end{pmatrix} + \begin{pmatrix} d_1 \\ d_2 \end{pmatrix}. \tag{40}$$

Using (40) $C_U(z)$ in (35) can now be rewritten as a function of A_L and B_L (implemented in **benthic_utils.xformsoln**)):

$$C_U(z) = (c_1 A_L + c_2 B_L + d_1) \cdot E_U(z) + (c_3 A_L + c_4 B_L + d_2) \cdot F_U(z) + G_U(z)$$

and hence define the "transformed" basis functions $E^*_U(z)$, $F^*_U(z)$, $G^*_U(z)$ such that:

$$C_U(z) = A_L \cdot E^*_U(z) + B_L \cdot F^*_U(z) + G^*_U(z) \tag{41}$$

where

$$\begin{aligned} E^*_U(z) &= c_1 E_U(z) + c_3 F_U(z) \\ F^*_U(z) &= c_2 E_U(z) + c_4 F_U(z) \\ G^*_U(z) &= G_U(z) + d_1 E_U(z) + d_2 F_U(z) \end{aligned} \tag{42}$$

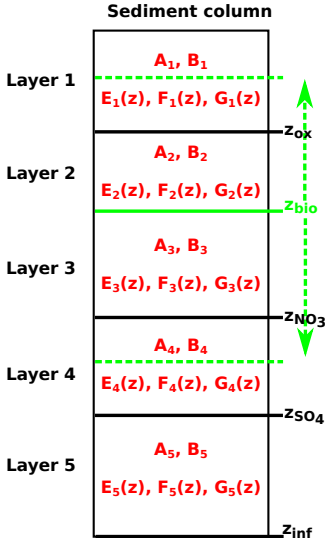

Figure 3. Schematic of the generic boundary condition matching (GBCM) problem. Showing the resulting integration constants (A_i, B_i) and ODE solutions (E_i, F_i, G_i) for the different sediment layers and the variable bioturbation boundary.

Equations (40), (41) and (42) can now be consecutively applied for each of the dynamic biogeochemical zone boundary, starting at the bottom of the sediment column. The net result is a piecewise solution of the whole sediment column with just two integration constants (coming from the lowest layer), which can then be solved for by applying the boundary conditions at the sediment-water interface and the bottom of the sediments .

Abstracting out the bioturbation boundary

The bioturbation boundary affects the diffusion coefficient of the modelled solutes, as well as the conservation equation of organic matter (and thereby the exact form of each reaction-transport equation). The boundary is particularly inconvenient as it can, in principle, occur in the middle of any of the dynamically shifting biogeochemical zones and therefore generates multiple cases (compare Fig. 3). The GBCM algorithm described above is thus not only used to construct a piecewise solution, but also to abstract out the bioturbation boundary. **This needs to be described better! Even I don't get this! For each timestep, the "bioturbation-status" of each biogeochemical zone (fully bioturbated, fully non-bioturbated or crossing the bioturbation boundary) is initially tested and (if needed) a piecewise solution is constructed by matching boundary conditions across the bioturbation boundary I don't think that this is clear to everyone. The routine zTOC.prepfg_l12 hands back a structure ls containing the "bioturbation-status" for each layer and (if needed) the description of the piecewise solution (coeffcients $c_1, c_2, c_3, c_4, d_1, d_2$ as above include direct reference here). For instance, in the case of sulfate, zTOC.prepfg_l12 is called three times before the actual profile is calculated (once per layer: oxic, nitrogenous, sulfidic) and hands back three structures ls with information about the layer's "bioturbation-status" and all associated conditional logic this is vague, be precise! what is handed back. When calculating the solutions for the different layers, the pre-calculated structure ls is passed to the function zTOC.calcfg_l12 which sorts out the correct solution type to use. The main code therefore never needs to know whether it is dealing with a piecewise solution (i.e. matched across a bioturbation boundary) or a "simple" solution (i.e. the layer is fully bioturbated or fully non-bioturbated)**.

2.4 Model Parameters

The following section provides a summary of global relationships used to constrain reaction and transport parameters in OMEN-SED. Table 9 synthesises sediment and transport parameters, while table 10 provides an overview of all biogeochemical parameters used in OMEN-SED.

2.4.1 Transport Parameters

The burial of sediments and porewater is directly related to the accumulation of new material on the seafloor (i.e. sedimentation, Burdige, 2006). This results in a downward advective flux of older sediment material and porewater in relation to the sediment-water interface. When coupled to an ocean model, its sedimentation flux can be readily used in OMEN-SED. The stand-alone version **is that the first time you mention stand-alone? this should be monetione in the general section- there is a stand alone** of OMEN-SED uses the empirical global relationship between sediment

accumulation rate (cm yr^{-1}) and seafloor depth (m) of Middelburg et al. (1997):

$$w = 3.3 \cdot 10^{-0.87478367 - 0.00043512 \cdot \text{depth}}, \tag{43}$$

As discussed before (Sec. **??**), the diffusion coefficient of species i is calculated as $D_i = D_{i,0} + D_{\text{bio}} = D_{\text{mol},i} \cdot f_{ir} + D_{\text{bio}}$ for dissolved species and $D_i = D_{\text{bio}}$ for solid species. The bioturbation coefficient D_{bio} (cm^2 yr^-1) is constant in the bioturbated zone and also follows the empirical relationship by Middelburg et al. (1997):

$$D_{\text{bio}} = 5.2 \cdot 10^{0.76241122 - 0.00039724 \cdot \text{depth}} \tag{44}$$

Observations indicate that bioturbation is largely restricted to the upper 10 cm of the sediments and is only marginally related to seafloor depth (e.g. Boudreau, 1998; Teal et al., 2010). Therefore, OMEN-SED imposes a globally invariant bioturbation depth z_{bio} of 10 cm. In case the bottom water oxygen concentration is below 5 nanomole cm^{-3} infaunnal activity is assumed to cease and $z_{\text{bio}} = 0.01$ cm **need to explain why not 0**.

Bioirrigation can enhance the molecular diffusion coefficient $D_{i,0} = D_{\text{mol},i} \cdot f_{ir}$ (Soetaert et al., 1996a). However, here we do not consider this effect and set f_{ir} to a constant value of 1. The specific molecular diffusion coefficients $D_{\text{mol},i}$ are corrected for sediment porosity ϕ, tortuosity F and are linearly interpolated for an ambient temperature T using zero-degree coefficients D_i^0 and temperature-dependent diffusion coefficients D_i^T (compare Gypens et al., 2008):

$$D_{\text{mol},i} = (D_i^0 + D_i^T \cdot T) \cdot \frac{1}{\phi \cdot F}$$

Tortuosity can be expresssed in terms of porosity as $F = \frac{1}{\phi^m}$ (Ullman and Aller, 1982) with the exponent m varying according to the type of sediment (here we use m=3). Values for D_i^T and D_i^0 are summarised in Table 9 and are adapted from Li and Gregory (1974) and Gypens et al. (2008).

2.4.2 Reaction Parameters and Stoichiometries

difficult to find a structure, I'd adapt to the order in the table and groups -as much as possible- according to chemical species, Also ALL parameters must be described and justified. **Let me take care of this section:** The first-order organic matter degradation constants of compound class i, k_i (yr^{-1}), are assumed invariant along the sediment column and therefore independent of the nature of the terminal electron acceptor. The rate constants can be altered manually to fit observed sediment profiles (compare Section 4.1) or related to a master variable (e.g. sedimentation rate or POC-flux) provided by a coupled Earth system model (compare Section 3.3.1 and 4.4). **until here, also need to mention** f_i Organic matter degradation consumes oxygen with a 1:1 stoichiometry.

N-related parameters: N/C, NO_3C, NH4, adsorption coefficient, gamma- explain nitrification SO4-H2S related parameters: SO_4C , gamma, AOM reduction of 1 mol organic matter additionally produces $SO_4C = \frac{138}{212}$ mol of hydrogen sulfide

Table 9. Sediment characteristics and transport parameters. TODO: PO4 adsorption coefficients okay?

Parameter	Unit	Value	Description/Source
ρ_{sed}	$\mathrm{g\,cm^{-3}}$	2.6	Sediment density
w	$\mathrm{cm\,yr^{-1}}$	Fct. of seafloor	Advection/Sediment accumulation rate
		depth or from ESM	(Middelburg et al., 1997)
z_{bio}	cm	10 or 0.01	Bioturbation depth
			(Boudreau, 1998; Teal et al., 2010)
D_{bio}	$\mathrm{cm^2\,yr^{-1}}$	Fct. of seafloor	Bioturbation coefficient
		depth	(Middelburg et al., 1997)
ϕ	-	0.85	Porosity
F	-	$\frac{1}{\phi^m}$	Tortuosity, here m=3
f_{ir}	-	1	Irrigation factor
Adsorption coefficients			
$K_{\mathrm{NH_4}}$	-	1.3	NH_4 adsorption coefficient, (see Wang and Van Cappellen, 1996)
$K^{\mathrm{ox}}_{\mathrm{PO_4}}$	-	200.0	PO_4 adsorption coefficient (oxic), (see Slomp et al., 1998)
$K^{\mathrm{anox}}_{\mathrm{PO_4}}$	-	1.3	PO_4 adsorption coefficient (anoxic), (see Slomp et al., 1998)
Diffusion coefficients (Li and Gregory, 1974; Schulz, 2006; Gypens et al., 2008)			
$D^0_{\mathrm{O_2}}$	$\mathrm{cm^2\,yr^{-1}}$	348.62	Molecular diffusion coefficient of oxygen at 0°C
$D^T_{\mathrm{O_2}}$	$\mathrm{cm^2\,yr^{-1}\,{}^\circ C^{-1}}$	14.09	Diffusion coefficient for linear temp. dependence of oxygen
$D^0_{\mathrm{NO_3}}$	$\mathrm{cm^2\,yr^{-1}}$	308.42	Molecular diffusion coefficient of nitrate at 0°C
$D^T_{\mathrm{NO_3}}$	$\mathrm{cm^2\,yr^{-1}\,{}^\circ C^{-1}}$	12.26	Diffusion coefficient for linear temp. dependence of nitrate
$D^0_{\mathrm{NH_4}}$	$\mathrm{cm^2\,yr^{-1}}$	309.05	Molecular diffusion coefficient of ammonium at 0°C
$D^T_{\mathrm{NH_4}}$	$\mathrm{cm^2\,yr^{-1}\,{}^\circ C^{-1}}$	12.26	Diffusion coefficient for linear temp. dependence of ammonium
$D^0_{\mathrm{SO_4}}$	$\mathrm{cm^2\,yr^{-1}}$	157.68	Molecular diffusion coefficient of sulfate at 0°C
$D^T_{\mathrm{SO_4}}$	$\mathrm{cm^2\,yr^{-1}\,{}^\circ C^{-1}}$	7.88	Diffusion coefficient for linear temp. dependence of sulfate
$D^0_{\mathrm{H_2S}}$	$\mathrm{cm^2\,yr^{-1}}$	307.48	Molecular diffusion coefficient of sulfide at 0°C
$D^T_{\mathrm{H_2S}}$	$\mathrm{cm^2\,yr^{-1}\,{}^\circ C^{-1}}$	9.64	Diffusion coefficient for linear temp. dependence of sulfide
$D^0_{\mathrm{PO_4}}$	$\mathrm{cm^2\,yr^{-1}}$	112.91	Molecular diffusion coefficient of phosphate at 0°C
$D^T_{\mathrm{PO_4}}$	$\mathrm{cm^2\,yr^{-1}\,{}^\circ C^{-1}}$	5.59	Diffusion coefficient for linear temp. dependence of phosphate
D^0_{DIC}	$\mathrm{cm^2\,yr^{-1}}$	151.69	Molecular diffusion coefficient of DIC at 0°C
D^T_{DIC}	$\mathrm{cm^2\,yr^{-1}\,{}^\circ C^{-1}}$	7.93	Diffusion coefficient for linear temp. dependence of DIC
D^0_{ALK}	$\mathrm{cm^2\,yr^{-1}}$	151.69	Molecular diffusion coefficient of ALK at 0°C
D^T_{ALK}	$\mathrm{cm^2\,yr^{-1}\,{}^\circ C^{-1}}$	7.93	Diffusion coefficient for linear temp. dependence of ALK

Note: DIC and ALK coefficients are the values of HCO_3^- from Schulz (2006).

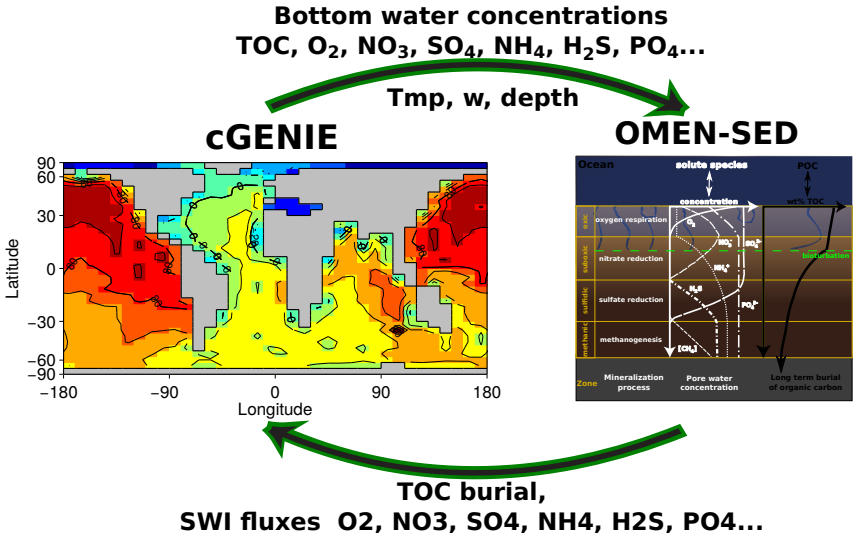

Figure 4. Schematic of the relationship between OMEN-SED and cGENIE. Arrows and accompanied text represent the information transferred between models.

methane: MC, AOM MC = 0.5 mol of methane.

The rate constants sorption of PO_4 to Fe oxides, k_s, release of PO_4 from Fe-bound P due to Fe-oxide reduction k_m and authigenic CFA precipitation k_a are constrained on the basis of ??. The pore water equilibrium concentrations for P sorption and CFA precipation (${PO_4}^s$, ${PO_4}^a$) and the asymptotic concentration for Fe-bound P (M^∞) are taken from Palastanga et al. (2011). The phosphorus to carbon ratio represents the composition of organic matter and is chosen as ?? based on ??.

See Table 10 for a complete summary of the parameters and their values.

3 Sensitivity Study & Case Studies working title, need to come up with something!

3.1 Sensitivity Study

3.2 Case Study: Stand-Alone simulations of global ocean transect

3.3 Case Study: Coupled pre-industrial Earth System Model Simulations

I wonder if we should not include a case Study section here, and if you should not provide technical details about the stand alone

Table 10. Values for biogeochemical parameters used in OMEN-SED. The variables x, y and z denote the atomic ratio of carbon, nitrogen and phosphorous of the degrading organic matter (here set to $C : N : P = 106 : 16 : 1$). P related coefficients okay?

Parameter/Variable	Unit	Value	Description
Stoichiometric factors and molecular ratios			
NC_i	mol/mol	$\frac{y}{x} = \frac{16}{106}$	nitrogen to carbon ratio
PC_i	mol/mol	$\frac{z}{x} = \frac{1}{106}$	phosphorus to carbon ratio
MC	mol/mol	0.5	methane to carbon ratio
			produced during methanogenesis
$DICC^{I}$	mol/mol	1.0	DIC to carbon ratio until z_{SO_4}
$DICC^{II}$	mol/mol	0.5	DIC to carbon ratio below z_{SO_4}
O_2C	mol/mol	$\frac{x+2y}{x} = \frac{138}{106}$	oxygen to carbon ratio
NO_3C	mol/mol	$\frac{4x+3y}{5x} = \frac{94.4}{106}$	nitrate to carbon ratio
SO_4C	mol/mol	$\frac{1}{2}O_2C = \frac{138}{212}$	sulfate to carbon ratio
ALK^{OX}	mol/mol	$\frac{y-2z}{x} = \frac{14}{106}$	ALK from aerobic degradation
ALK^{NIT}	mol/mol	-2	ALK from nitrification
ALK^{DEN}	mol/mol	$\frac{4x+3y-10z}{5x} = \frac{92.4}{106}$	ALK from denitrification
ALK^{SUL}	mol/mol	$\frac{x+y-2z}{x} = \frac{120}{106}$	ALK from sulfate reduction
ALK^{MET}	mol/mol	$\frac{y-2z}{x} = \frac{14}{106}$	ALK from methanogenesis
ALK^{H2S}	mol/mol	-2	ALK from H_2S oxidation
ALK^{AOM}	mol/mol	2	ALK from AOM
Secondary reaction parameters			
γ_{NH_4}	-	0.9	fraction of NH_4 that is oxidised
			in oxic layer
γ_{H_2S}	-	0.95	fraction of H_2S that is oxidised
			in oxic layer
γ_{CH_4}	-	0.99	fraction of CH_4 that is oxidised
			at z_{SO_4}
P related parameters			
k_s	yr^{-1}	1.0	Rate constant for PO_4 sorption
k_m	yr^{-1}	0.02	Rate constant for Fe-bound P release
k_a	yr^{-1}	10.0	Rate constant for authigenic CFA precipitation
${PO_4}^s$	$mol\,cm^{-3}$	$1 \cdot 10^{-9}$	equilibrium conc. for P sorption
			(Slomp et al., 1996)
${PO_4}^a$	$mol\,cm^{-3}$	$3.7 \cdot 10^{-9}$	equilibrium conc. for authigenic P precipitation
			(Slomp et al., 1996)
M^{∞}	$mol\,cm^{-3}$	$1.99 \cdot 10^{-10}$	asymptotic concentration for Fe-bound P
			(Slomp et al., 1996)

DH: ALK^{OX} correct?: y=NH4 prod.; -2z=P release

3.3.1 Coupling to an Earth System Model

OMEN-SED is coupled to the carbon-centric version of the "GENIE" Earth system model (cGENIE Ridgwell et al., 2007) to illustrate the abilities of the newly developed model. The following section provides a brief description of cGENIE and the

is described (Fig. 4). Results from pre-industrial experiments are presented in Section 4.4. cGENIE is a model of Intermediate Complexity based on the efficient climate model "C-GOLDSTEIN" of Edwards and Marsh (2005), featuring a frictional-geostrophic 3D-ocean circulation model coupled to a fast Energy-Moisture Balance 2D-atmosphere together with a dynamic-thermodynamic sea-ice component. The version of cGENIE used here includes the marine geochemical cycling of carbon, oxygen, phosphorus and sulfur (Ridgwell et al., 2007), preservation of carbonates in deep-sea sediments (Ridgwell and Hargreaves, 2007) and terrestrial weathering (Colbourn et al., 2013). The ocean model is implemented on a 36×36 equal-area horizontal grid with 16 vertical levels using the pre-industrial continental configuration and bathymetry as in Archer et al. (2009). In contrast to Archer et al. (2009) the same grid resolution (36×36) is used for the sediment geochemistry model SEDGEM. Instead of completely degrading POC at the seafloor, OMEN-SED is called by SEDGEM for each wet ocean grid point. Depending on the overlying biogeochemical ocean model, processes can be included or excluded in OMEN-SED and stoichiometric factors need to be adjusted to ensure preservation of mass. As nitrogen is not modelled explicitly in the employed cGENIE configuration the related stoichiometries in OMEN-SED are set to zero (i.e. $\mathrm{NC_i}$, $\mathrm{ALK^{NIT}}$ and $\mathrm{ALK^{DEN}}$). cGENIE, however, implicitly includes the effects of $\mathrm{NH_4}$ release and its nitrification on Alkalinity and neglects the impact of P release; therefore, related stoichiometries are changed to $\mathrm{ALK^{OX}} = -16/106$ and $\mathrm{ALK^{SUL}} = 122/106$.

Several biogeochemical tracers and parameters are transferred from SEDGEM to OMEN-SED and have to be converted into the required units. Bottom water concentrations of solutes are converted from $\mathrm{mol\,kg^{-1}}$ to $\mathrm{mol\,cm^{-3}}$ and the depositional flux of POC ($\mathrm{POC_{flux}}$) is converted from $\mathrm{cm^3\,cm^{-2}\,yr^{-1}}$ to $\mathrm{mol\,cm^{-2}\,yr^{-1}}$ assuming an average density of POC of $1.0\,\mathrm{cm^3\,g^{-1}}$. Other parameters used from cGENIE are seafloor depth, local temperature and the partitioning of bulk POC into the slower and faster degrading pool (as cGENIE represents a labile and a refractory POC fraction, see Ridgwell et al. (2007)). The advection/sediment accumulation rate is generally taken from cGENIE, however, a minimum value of $w = 0.5\,\mathrm{cm\,kyrs^{-1}}$ is imposed as OMEN-SED tends to be unstable for lower values. The bulk $\mathrm{POC_{flux}}$ is seperated into the labile and refractory component and the routine to calculate the sedimentary POC profiles is called. Here, the two POC depositional fluxes are first converted into SWI concentrations (in $\mathrm{mol\,cm^{-3}}$) by solving Eq. (2) for z=0. OMEN-SED computes the resulting SWI-fluxes of solutes (in $\mathrm{mol\,cm^{-2}\,yr^{-1}}$) and the fraction of POC preserved in the sediment at a depth of 100 cm ($\mathrm{POC_{pres}}$) and returns the results to cGENIE. In case no POC is deposited on the seafloor (i.e. $\mathrm{POC_{flux}} = 0$), OMEN-SED is not called and the SWI-fluxes of solutes and $\mathrm{POC_{pres}}$ are set to zero. In order to reduce memory requirements the sediment profiles

(e.g. as shown in Fig. 5) are not calculated in the FORTRAN version of OMEN-SED, however, the boundary conditions are saved at the end of the experiment and sediment profiles for specific grid-cells, ocean basins and/or ocean transects can be plotted using the stand-alone MATLAB version of OMEN-SED.

4 Model Applications

To validate our approach, model results were compared with observed pore water profiles (Section 4.1), an extensive sensitivity analysis for the most important model parameters was performed and resulting sediment-water interface fluxes were compared with a global database (Section 4.2). Furthermore, OMEN-SED was coupled to the cGENIE Earth system model and different published parameterisations for the OM degradation rate constants are tested on a global scale (Section 4.4).

4.1 Sediment profiles

Modelled profiles were compared with measured pore water data from different ocean depths (Figure 5) including the continental shelf (108 m), upper slope (585 m), lower slope (2213 m) and the deep sea (4298 m). The site at 585 m depth located in the Santa Barbara Basin is characterised by anoxic bottom waters and high POC concentrations (POC ∼5.5 wt%, Reimers et al., 1996), whereas the other sites at the Iberian margin (108 and 2213 m) and the Nazaré Canyon (4298 m, Epping et al., 2002) are oxic. Sediment-water interface characteristics and concentrations of POC and dissolved species in OMEN-SED were set to the observed values where available (Table 11). The POC and pore water profiles were fitted by optimizing the POC partitioning into the fast and slow degrading pool and their respective first order degradation rate constants (priority given to reproduce the POC and O_2 profiles). For phosphorus the equilibrium concentration for authigenic P formation (PO_4^a) was adjusted to fit the PO_4 concentration at z_∞. For the two open Iberian margin stations (108 and 2213 m) OMEN-SED fits all observations well. OMEN-SED does especially well at depth 2213m by reproducing the deep O_2 penetration and the subsurface maximum in NO_3 concentration due to the nitrification of NH_4. For the Santa Barbara basin (585 m) a misfit is observed for H_2S and PO_4 in the upper 20 cm of the sediment. This can be explained by the presence of Mn^{2+}, Fe^{2+} and dissolved Fe at this site which are either reduced to degrade POC and/or react with H_2S to form iron sulfides, therefore inhibiting the rise in concentration of H_2S (Reimers et al., 1996). Phosphorus is adsorbed to Fe oxides and incorporated into carbonate fluorapatite (CFA) which is highly parameterised in OMEN-SED and not modelled explicitly. For the Nazaé Canyon station (4298 m) satisfactory fits could be realised apart from NH_4. However, also the original study (Epping et al., 2002) had the same problem using a more complex diagenetic model and suggested non-local solute exchange being responsible for the higher NH_4 concentrations at this site.

DH: P explanation correct/okay? Also, say something about [ALK] at 585m?

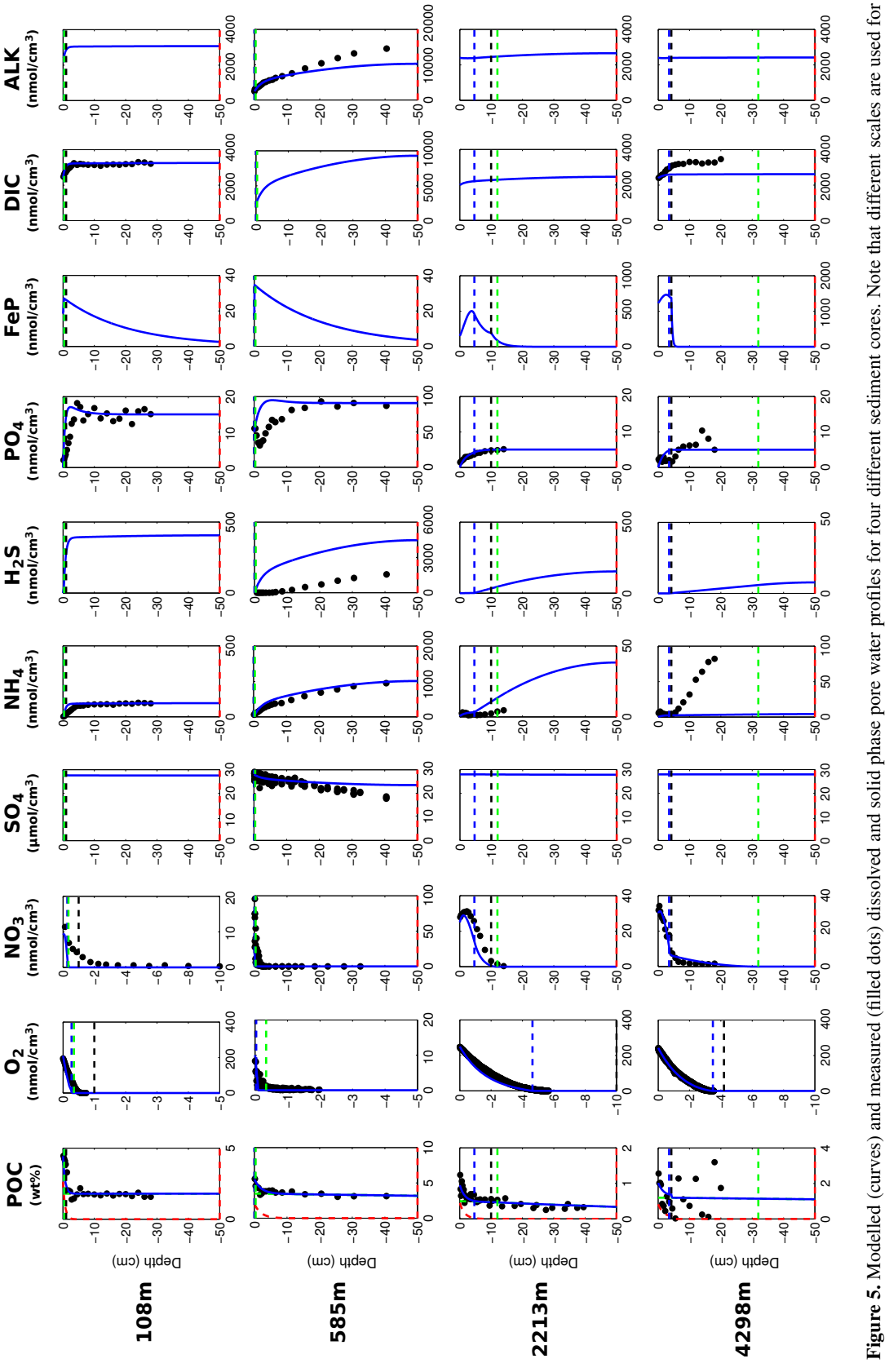

Figure 5. Modelled (curves) and measured (filled dots) dissolved and solid phase pore water profiles for four different sediment cores. Note that different scales are used for different stations. The blue POC curve represents the sum of the refractory (green) and labile (red) POC fraction.

Table 11. Model boundary conditions for the sampling stations in Figure 5. (For all sites DIC bottom water concentration of 2,400 nanomole cm^{-3} is assumed.)

Sediment characteristics:								
Depth (m)	Temp. ($^{\circ}C$)	z_{bio} (cm)	D_{bio} (cm^{2}yr^{-1})	POC_1 (wt%)	POC_2 (wt%)	k_1 (yr^{-1})	k_2 (yr^{-1})	
108	12.5	1.0	0.02	2.64	1.8	0.65	$1.0e^{-5}$	
585	5.85	0.01	0.02	2.0	3.5	0.2	$8.0e^{-4}$	
2213	3.2	10.0	0.17	0.45	0.5	0.1	$4.0e^{-4}$	
4298	2.5	4.2	0.18	0.83	1.2	0.052	$1e^{-5}$	
Bottom water concentrations of solutes (all in nanomole cm^{-3}):								
Depth	O_2	NO_3	SO_4	NH_4	H_2S	PO_4	PO_4^a	Alkalinity
108	210	9.6	28,000	0.4	0.0	0.0	15.0	2,400
585	10	25.0	28,000	0.0	0.0	50.0	90.0	2,480
2213	250	25.0	28,000	0.6	0.0	0.0	5.0	2,400
4298	243	30.1	28,000	0.22	0.0	0.0	5.0	2,400

4.2 Sensitivity Analysis

Model parameters implicitly account for processes not explicitly described, they are notoriously difficult to constrain and a source of uncertainty for numerical and analytical models. One strategy to explore and quantify this model uncertainty that can always be applied is sensitivity analysis (SA). SA is a term used for mathematical techniques to investigate how the variations in the outputs (y_1, ..., y_N) of a model can be attributed to variations in the different input parameters (x_1, ..., x_M) (Pianosi et al., 2016). Different types of sensitivity indices, which quantify this relative influence with a scalar S_i, can be calculated, ranging from simple one-at-a-time methods to statistical evaluations of the output distribution (e.g. variance-based or density-based approaches Pianosi et al., 2016). Especially the latter indices are easy to interpret and can be compared across different parameters and/or different model outputs as they generally take values between zero and one ($S_i \in [0, 1]$). An index of zero indicates a non-influential parameter and a higher value a more influential parameter. Here, we use SA mainly to identify which parameters have the largest impact on the different model outputs and therefore require careful calibration. As the probability density functions of our model outputs (i.e. the resulting SWI-fluxes) are generally highly-skewed towards extreme organic matter degradation rates (not shown) variance-based sensitivity indices are not very reliable uncertainty indicators (Pianosi et al., 2016). Rather than just considering the variance we employ the novel density-based PAWN method by Pianosi and Wagener (2015) which considers the entire conditional and unconditional Cumulative Destribution Function (CDF) of the model output. The sensitivity

index of parameter i is calculated as the difference between the two CDFs, i.e.

$$S_i = \max_{x_i} \max_{y} |F_y(y) - F_{y|x_i}(y)| \tag{45}$$

where $F_y(y)$ is the unconditional CDF of the output y and $F_{y|x_i}(y)$ represents the conditional CDF when the i-th parameter is fixed to x_i. For a more detailed description of the method we refer the interested reader to Pianosi and Wagener (2015).

Due to the model complexity it is impossible to compute the sensitivity indices analytically therefore they are approximated from a Latin-Hypercube sampling of parameter inputs and calculated outputs. The PAWN method, as implemented within the Sensitivity Analysis for Everyone (SAFE) MATLAB toolbox (Pianosi et al., 2015), is used to investigate 11 model parameters for ranges as specified in Table 12. Sensitivity indices for all resulting SWI-fluxes for two idealised sediment conditions (i.e. anoxic at 400 m and oxic at 4000 m, see Table 13) are calculated. We use 200 samples to estimate the unconditional CDF, 100 samples to estimate the conditional CDFs and 10 conditioning points, thus 11,200 evaluations are performed for each sediment condition. The resulting indices (compare Fig. 10 in the Appendix) are then translated into a color code and summarised in a pattern plot to simplify comparison (Fig. 6). The most significant parameters for all model outputs are the degradation rate for the labile OM part ($\mathrm{k_1}$) and its share in the total OM pool ($\mathrm{f_1}$). For the anoxic setup, where no oxidation occurs, the secondary redox parameters (i.e. $\gamma_{\mathrm{NH_4}}$, $\gamma_{\mathrm{H_2S}}$) are essentially non-influential. Whereas in the oxic scenario, SWI-fluxes of $\mathrm{NH_4}$, $\mathrm{SO_4}$ and $\mathrm{H_2S}$ are very sensitive to changes in the secondary redox parameters. The $\mathrm{PO_4}$ SWI-flux appears to be insensitive especially under for the oxic condition as the majority is absorbed to Fe-oxides. The sensitivities change if other $\mathrm{PO_4}$ related equilibrium concentrations ${\mathrm{PO_4}}^s$, ${\mathrm{PO_4}}^a$ and M^∞ are used (not shown).

DH: explanation for small P sensitivity correct?

To test if OMEN-SED is able to reproduce the magnitude of observed SWI-fluxes, another set of Latin-Hypercube samplings is produced for the two idealised sediment conditions (sample sizes $N = 3500$) . Here just the two most sensitive parameters $\mathrm{k_1}$ and $\mathrm{f_1}$ and also $\widetilde{\mathrm{k_2}}$ are varied, the other parameters are set to their default values (Tables 9 and 10). For the deep sea condition we account for the presence of more refractory OM by sampling $\mathrm{f_1} \in [0.02, 0.3]$. Minimum and maximum values for $\mathrm{k_1}$, $\widetilde{\mathrm{k_2}}$ and $\mathrm{f_1}$ in the shallow ocean are as in Table 12. The results are compared with a global database of benthic fluxes of $\mathrm{O_2}$ and $\mathrm{NO_3}$ (Bohlen et al., 2012). The coloured scatter plots in Figure 7 show that the observed fluxes fall well in the range of SWI-fluxes calculated with OMEN-SED. Also highlighted by the emergence of colour patterns in Figure 7 A+B are the strong interactions between the amount of labile OM $\mathrm{f_1}$ and its degradation rate $\mathrm{k_1}$ for the resulting SWI-fluxes of the most powerful TEA available. In general, a higher degradation rate in combination with more labile OM available leads to a higher SWI-flux.

Table 12. Range of model parameters used for sensitivity analysis of model predicted output.

Parameter	Description	Units	Minimum	Maximum	Source
k_1	labile OM degradation constant	yr^{-1}	$1e^{-4}$	5.0	(1)
$\widetilde{k_2}$	order of refractory OM degradation constant ($k_2 = \widetilde{k_2} \cdot k_1$)	-	$1e^{-4}$	$1e^{-1}$	(1)
f_1	fraction of labile OM	-	0.02	0.98	-
K_{NH_4}	Adsorption coefficient	-	0.8	1.7	(2)
γ_{NH_4}	NH_4 fraction oxidised		0.5	1.0	-
γ_{H_2S}	H_2S fraction oxidised		0.5	1.0	-
$K^{ox}_{PO_4}$	Adsorption coeff. oxic	-	100.0	400.0	(3)
$K^{anox}_{PO_4}$	Adsorption coeff. anoxic	-	1.3	2.0	(3)
k_s	kinetic P sorption	yr^{-1}	0.1	100.0	(4, 5)
k_m	Fe-bound P release	yr^{-1}	0.015	0.02	(4, 5)
k_a	authigenic P formation	yr^{-1}	0.001	10.0	(4, 6)

Sources: (1) Arndt et al. (2013); (2): Van Cappellen and Wang (1996); (3): Krom and Berner (1980) (4): Gypens et al. (2008); (5): Slomp et al. (1996); (6): Van Cappellen and Berner (1988)

Table 13. Model boundary conditions for the two idealised sediment conditions used for the sensitivity analysis (Fig. 6 and 7). All solute concentrations are in nanomole cm^{-3}.

Depth (m)	Temp. (°C)	OC (wt%)	O_2	NO_3	SO_4	PO_4	z_{bio} (cm)
400	8.0	2.0	0.0	40.0	28,000	40.0	0.001
4000	1.5	1.0	300.0	20.0	28,000	40.0	10.0

4.3 Global Hypsometric Analysis of TEA Fluxes

In this section we test to which degree OMEN-SED is capable of capturing the dynamics of organic matter degradation pathways and related TEA-fluxes as simulated with a complete, numerical diagenetic model. Therefore, we reproduce the simulations of typical conditions along a global ocean hypsometry of Thullner et al. (2009). To explore the global remineralisation of OM in the seafloor Thullner et al. (2009) quantified various diagenetic processes using the Biogeochemical Reaction Network Simulator (BRNS, Aguilera et al., 2005). In their study many model parameters (e.g. w, D_{bio} or ϕ) are related to the master variable seafloor depth (SFD) using existing empirical relationships. Organic matter degradation is described with a 1-G approach and the first order rate constant follows the empirical relationship of Boudreau (1997): $k = 0.38 \cdot w^{0.59}$. BRNS simulations were performed using boundary conditions and parameters for representative SFD of 100m, 200m, 500m, 1000m, 2000m, 3500m and 5000m. In order to reproduce these results, OMEN-SED is configured as a 1-G model and boundary conditions and model parameters are defined as given in Table 3 of (Thullner et al., 2009). As OMEN-SED assumes a fixed fraction of reduced substances to be re-

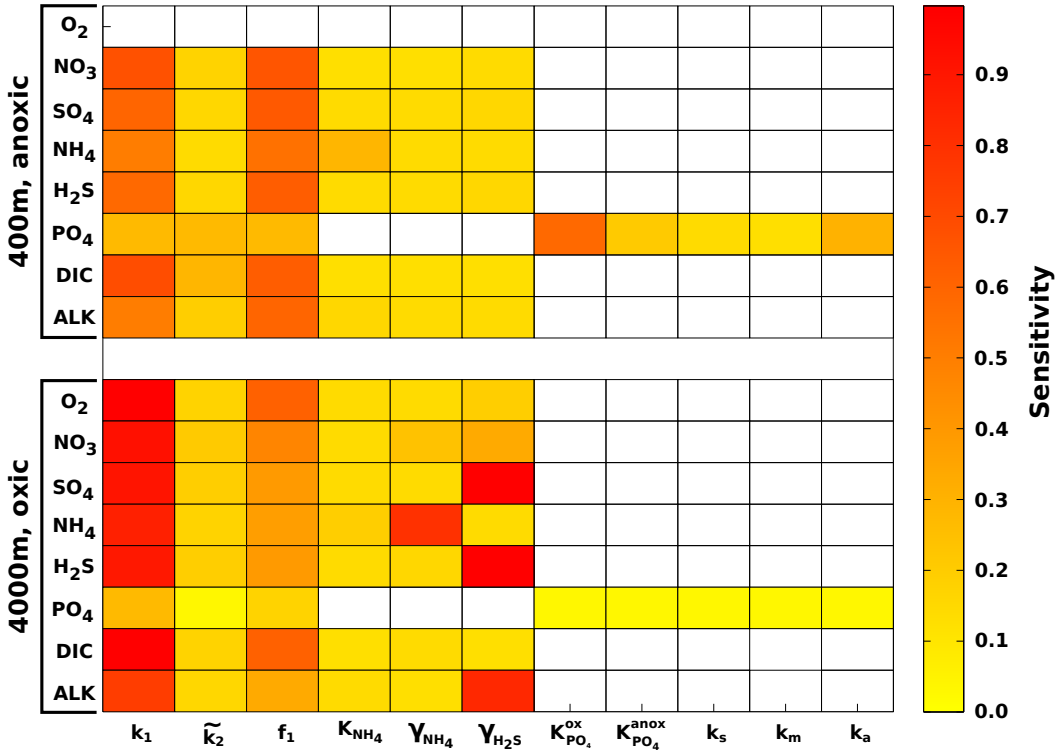

Figure 6. Pattern plot, showing the output sensitivity for each SWI flux (i.e. the chemical compounds on the vertical axis) and each input factor (i.e. the model parameters on the horizontal axis) for two idealised sediment cores. White patterns are assigned where the SWI flux is independent of the specific parameter.

DH: Rather low PO4 sensitivity - bc of Equil. concentr.?

oxidised which exerts a large impact on the resulting SWI-fluxes (compare Section 4.2) we perform two sets of simulations in order to show the range of possible model outputs. In the first setup 95% of the reduced substances are re-oxidised (i.e. $\gamma_{NH_4} = \gamma_{H_2S} = 0.95$) and in the second only 5% are re-oxidised (all other model parameters and boundary conditions are equal).

Figure 8 compares simulated SWI-fluxes of TEAs (i.e. O_2, NO_3 and SO_4) along the global hypsometry using OMEN-SED (black lines) with the results of Thullner et al. (2009) (red lines). Observations for O_2 and NO_3 fluxes are taken from Middelburg et al. (1996). Also plotted in Fig. 8A are the total oxygen uptake (TOU) estimates of Thullner et al. (2009) (filled red symbols), who assumed the organic matter flux to be equivalent to TOU. Considering the spatial variability in available data, Figure 8 shows that OMEN-SED is capable of reproducing the major observed trends in depth distributions of TEA fluxes. In general, fluxes calculated with BRNS fall within the range of possible OMEN-SED results (with the exception of NO_3 in the shallow ocean). In particular, the observed O_2 fluxes in the upper 2000m are well predicted by the two OMEN-SED simulations (Fig. 8A). Oxygen fluxes for the deep-sea sediments, however, are slightly underestimated. These deviations

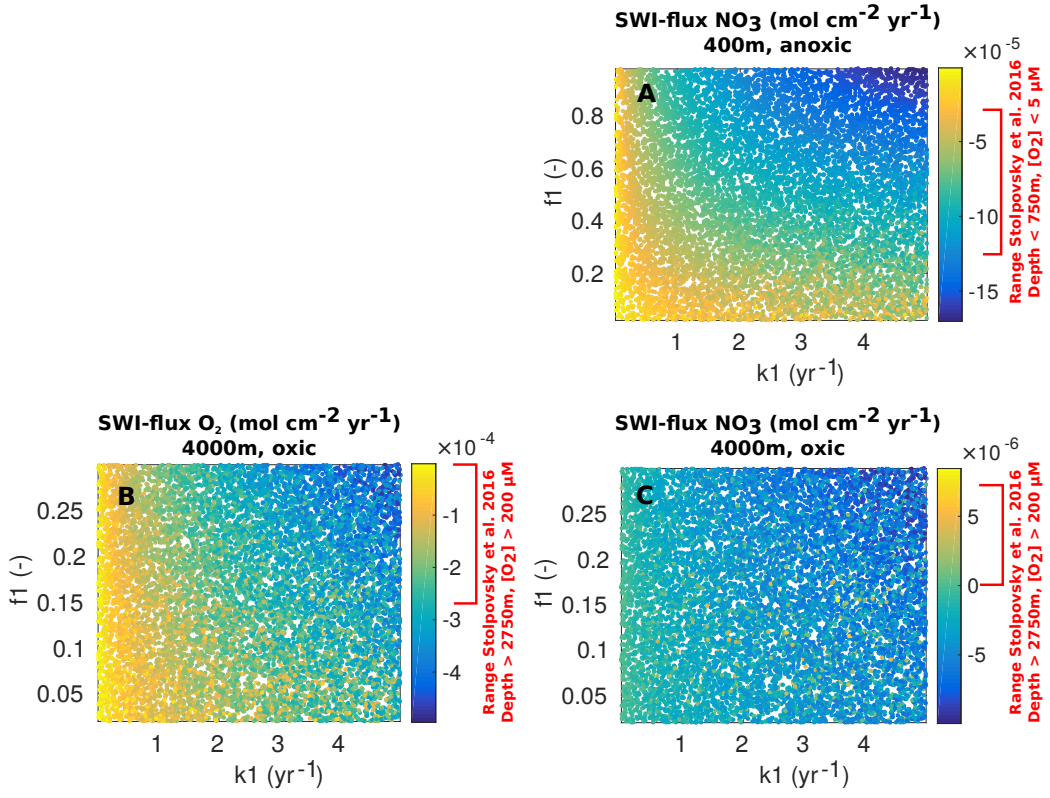

DH: Why mainly negative NO3-flux 4000m in contrast to database!?... might change when using diff. gamma

Figure 7. Coloured scatter plots (k_1 vs f_1) of resulting OMEN-SED SWI-fluxes for the 400m anoxic (A: NO_3) and 4000m oxic (B: O_2, C: NO_3) scenario. Negative values representing a flux from the water column into the sediments. Indicated area in red at the respective colour scale represents the range of benthic fluxes in the global database of Bohlen et al. (2012).

can presumably be related to the assumed 1-G description of organic matter degradation, which neglects the more labile OM pool. This highly reactive pool is degraded close to the sediment surface, thus promoting higher aerobic degradation rates and higher O_2 fluxes. Nitrate fluxes in the upper 500m of the Atlantic Ocean are well predicted. However, as in Middelburg et al. (1996) the direction of calculated nitrate fluxes in the upper 1000m of the Pacific Ocean differ from the observations. Middelburg et al. (1996) related these discrepancies to the globally averaged model parameters and the applied boundary conditions. They could reduce the disagreements significantly by using more representative bottom water concentrations for the eastern Pacific and a higher flux of labile organic matter for their 2-G model. By changing the boundary conditions and the NC-atomic ratio of organic matter for the whole hypsometry, it is possible to obtain a better model-data fit with OMEN-SED for the shallow Pacific Ocean (green line in Fig. 8B). Following Bohlen et al. (2012), who could show that the atomic NC-ratio strongly deviates from Redfield stoichiometry (0.151) with specifi-

cally lower values for the East Pacific Ocean, we adopt their globally averaged value of 0.067. In addition, bottom water conditions are changed to low oxygen/high nitrate levels more likely to be found in the shallow Pacific Ocean ($O_2 = 10$ nanomole cm^{-3} and $NO_3 = 80$ nanomole cm^{-3}).

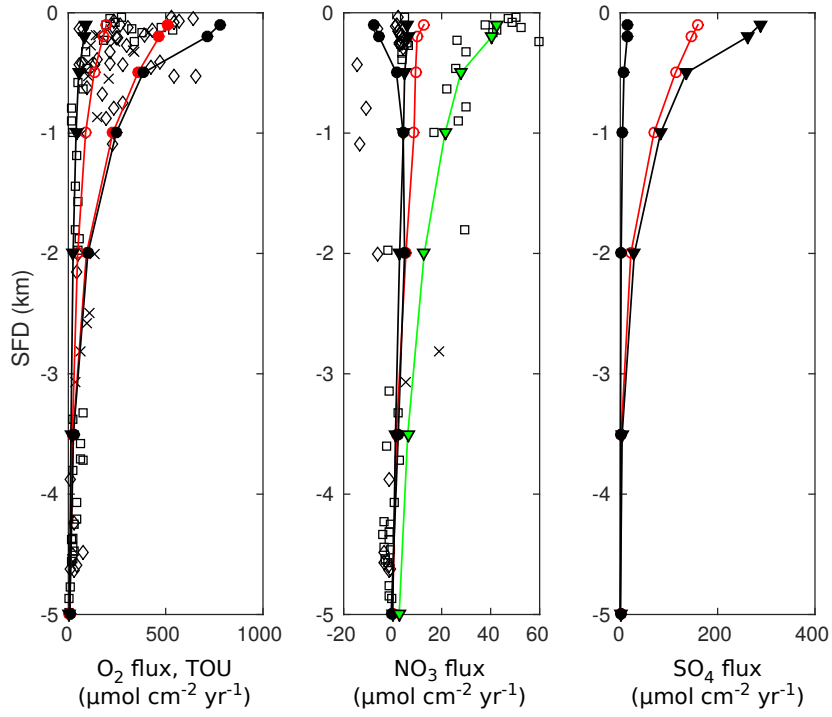

Figure 8. Fluxes of O_2, NO_3 and SO_4 to the sediment along the global hypsometry. Red lines (with open symbols) are modelled fluxes from Thullner et al. (2009) using BRNS; black lines are results from OMEN-SED (●: $\gamma_{NH_4} = \gamma_{H_2S} = 0.95$; ▼: $\gamma_{NH_4} = \gamma_{H_2S} = 0.05$). Observations of TEA fluxes are taken from Middelburg et al. (1996) (◊: Atlantic, □: Pacific, ×: Arctic/Indian Ocean). Also plotted in Figure (A) are the total oxygen uptake (TOU) estimates of Thullner et al. (2009) (filled red symbols). The green line indicates OMEN-SED results for low oxygen/high nitrate levels and the lower NC-ratio. Negative values are directed out of the sediments.

4.4 Pre-industrial cGENIE coupling and the OM degradation rate

OMEN-SED has been coupled to the global Earth system model cGENIE as described in Section 3.3.1. Our objective is not to perform and discuss a detailed calibration of the two models, as this is beyond the scope of this model development paper. We rather want to showcase, that a coupling is possible and the results show main sediment features one would expect to see on a global scale. All simulations are run for 20,000 years to steady-state. OMEN-SED is called for each grid-cell in every time step, feeding back the resulting SWI-fluxes and the fraction of POC preserved in the sediments to cGENIE.

Table 14. List of coupled OMEN-cGENIE experiments with oxic and anoxic rate constants (k_1, yr^{-1}). The rate constant k_2 for the more refractory component is calculated as $k_2 = k_1/100$, apart from the Control experiment where $k_2 = 1.0$. D: seafloor depth.

Experiment	oxic rate constant	anoxic rate constant	Reference/Description
Control	1.0	1.0	All OM is degraded
Tromp	$2.97 \cdot w^{0.62}$	$0.057 \cdot w^{1.94}$	Tromp et al. (1995)
Boudreau_Toth	$0.38 \cdot w^{0.59}$	$0.04 \cdot w^2$	Boudreau (1997) oxic
			Toth and Lerman (1977) anoxic
Stolpovsky_Toth	$1.02 \cdot w^{0.5}$	$0.04 \cdot w^2$	Stolpovsky et al. (2015) oxic
			Toth and Lerman (1977) anoxic
Palastanga	0.01	0.008	$D \leq 2000$ Palastanga et al. (2011)
	0.005	0.002	$D > 2000$ Palastanga et al. (2011)

As shown in our sensitivity analysis (Figure 6) and discussed by Arndt et al. (2013) the degradation rate constants for OM (k_i) are the most influential parameters and strongly determine the SWI-flux of redox-sensitive elements. Yet, their spatial variability is unknown at the global scale and reported rate constants can vary by almost 10 orders of magnitude (Arndt et al., 2013), thus defining appropriate OM degradation rate constants is a major challenge and source of uncertainty for diagenetic models. The rate constants in models are either determined through profile fitting for a specific site or, for global applications, they are related to a single, readily available characteristic (or master variable) of the local environmental conditions. For instance, considerable effort has been expended to relate the apparent rate constant for oxic and anoxic OM degradation to sedimentation rate (w) and various empirical relations have been proposed (Toth and Lerman, 1977; Tromp et al., 1995; Boudreau, 1997; Stolpovsky et al., 2015). Nevertheless, these relationships are generally based on limited data sets and their global applicability is questionable (Arndt et al., 2013). We test globally invariant values for the OM degradation rate constants as well as different published parameterisations (see Table 14) to test whether the different approaches are able to recreate main sediment characteristics. Depending on oxygen concentration in the bottom water, k_1 is defined as the oxic or anoxic degradation rate (anoxic for $[O_2] < 5$ nanomole cm^{-3}). The more refractory component is assumed to degrade one hundred times slower ($k_2 = k_1/100$, see e.g. Boudreau, 1997).

Describe Figure 9 and compare with what we know. E.g. Thullner et al. 2009!

Schulz and Zabel: The basic mechanism inducing microbial activity is the supply of organic matter to the seafloor and this is generally coupled to surface water produc- tivity. Most of the highly productive areas in the global ocean are adjacent to the continents, so that we can expect a decrease of degradation inten- sity from the coastal marine environments over the continental shelves and slopes into the deep- sea. This becomes evident when we look at the data compiled by Middelburg

et al. (1993) which indicate that 83% mineralisation and 87% burial in marine sediments occurs in the coastal zone occupying only 9% of the total ocean area. This means that the sediments with the highest respi- ration rates also have the highest burial efficiency in marine environments. Fluxes of oxygen and nitrate, therefore, vary over several orders of magnitude between oligo- trophic open ocean areas and continental shelf and slope areas. This is about 50 to 6,000 mmol m -2 yr -1 for oxygen and -600 to 380 mmol m -2 yr -1 for nitrate ...

(SHOW O2, NO3 AND E.G. PO4 SWI-fluxes).

Could also plot Figure 4 from Palastanga et al. (2011) with POC wt% for different sites in the ocean! UNITS of Fe-P! This is a solid! Therefore not nmol/cm3 rather mol/g as in Palastanga...

Also check what water column features to show and maybe sediment P or Fe-P concentrations (see PALASTANGA et al. 2011, 2013).

Stolpovsky: bioturbated sediments deposited at continental margins quickly become anoxic within a few millimeters [Wenzhöfer and Glud, 2002].

5 Scope of applicability and model limitations

State-of-the art numerical models representing the full complexity of the diagenetic processes typically perform adequately at reproducing site-specific biogeochemical dynamics, however, tuning model parameters is laborious, the computational demand is high and, thus, their transferability to the global scale is limited. On the other hand, analytical models are very efficient, but existing approaches coupled to global models generally use highly simplified reaction networks, often restricted to oxic degradation with a limited number of explicit pore water tracers. However, our ability to assess the role of organic matter dynamics for global biogeochemical cycles and climate requires tools that resolve the most important biogeochemical processes and tracers explicitly, while at the same time are computationally efficient and have a degree of predictive capability to extrapolate knowledge to data poor areas. The new model OMEN-SED presented here is a legitimate compromise between complexity of biogeochemical processes and computational efficiency. Its scope of applicability covers the entire range from regional to global scales. OMEN-SED's computational efficiency facilitates its use in two very different ways. Firstly, it can be coupled to global Earth system models and therefore allows the investigation of coupled global biogeochemical dynamics over different timescales. Secondly, it can be used to calculate quantitative sensitivity indices requiring large sample sizes such as variance- or density-based approaches. Therefore, OMEN-SED can help to quantitatively investigate how systematic variations in model parameters impact the model output, for instance when the model has been tuned to a site-specific problem. Due to the represented anaerobic processes and secondary-redox reactions, OMEN-SED is also useful to investigate the role of benthic-pelagic coupling on the development of ocean anoxia and euxinia for instance during

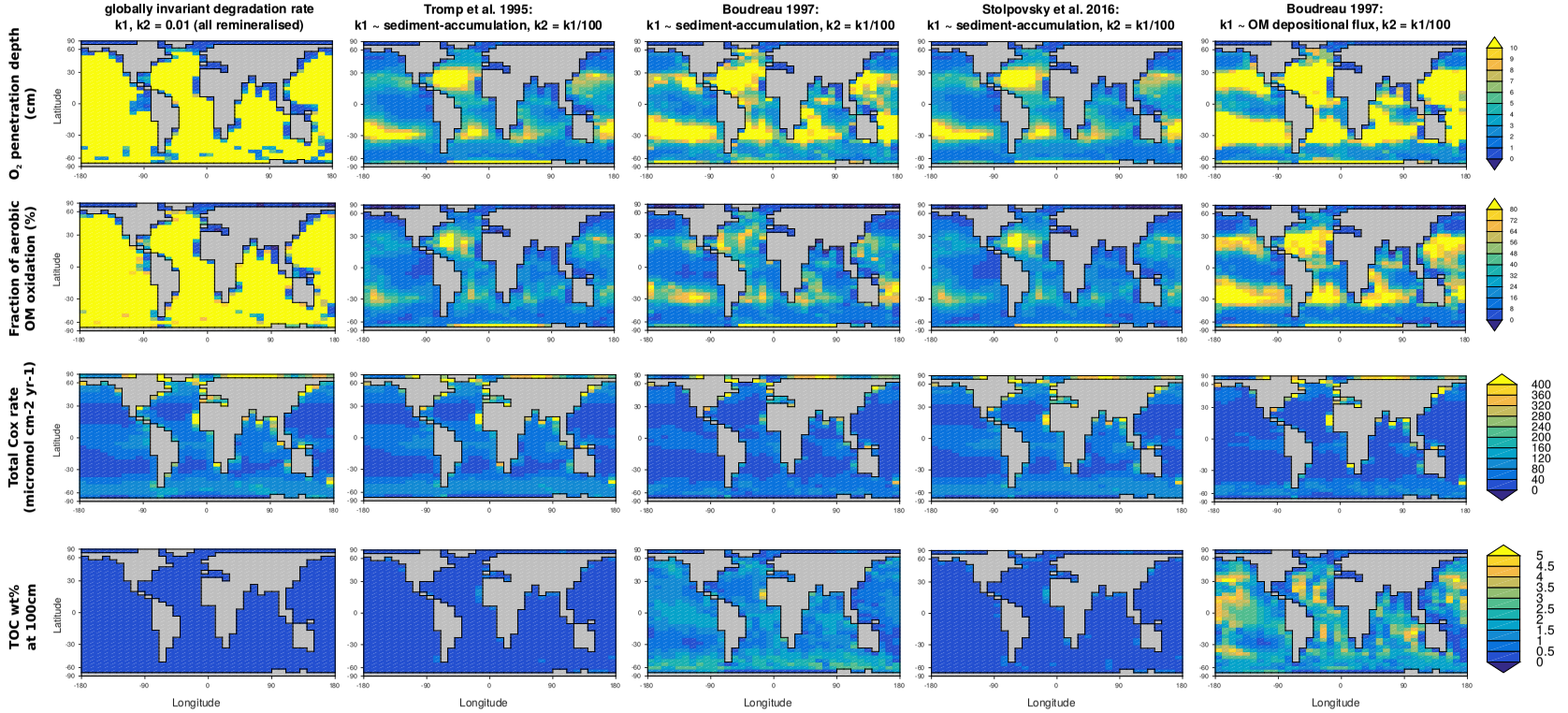

Figure 9. Results of OMEN-cGENIE coupling using different, published parameterisations for the OM degradation rates (k_1, k_2, compare Table **??**) coupled to the same cGENIE ocean setup. All results shown are sediment characteristics calculated by OMEN-SED. NOTE: Preliminary results (here frac2 still constant!) TODO: plot wt% just until 3%.

extreme climate events such as OAEs. On more regional scales it can be applied to systems like continental margins or estuaries which are characterised by complex interactions between different pathways of organic matter degradation and redox reactions. Here, the model can help to disentangle the complex process interplay that drives the biogeochemical dynamics and give quantifications for upper and lower constraints of carbon and nutrient budgets for these dynamic systems. In addition, OMEN-SED can be used to model eutrophication processes in shallow coastal waters as sediment-water oxygen and nutrient exchange fluxes are explicitly modelled and depend on re-oxidation of reduced substances which causes a substantial part of oxygen consumption in these environments.

However, the model presented here, even more complete than previous analytical models, is still associated with a certain degree of simplifications. In order to solve the diagenetic equation analytically important assumptions have been made, which limit the general applicability of the model. One of the most important simplifications is assuming steady-state. When coupled to an Earth system model this assumption is only valid if the relevant variability in boundary conditions and fluxes is generally longer than the characteristic timescales of the reaction-transport processes. In that case the sediment column can be described by a series of pseudo steady-states as it is done in OMEN-SED. Consequently, the model can be used for investigating the long term effects of changes in boundary conditions such as the the input of OM or bottom water oxidation state on degradation and burial dynamics, as for instance during OAEs. Yet, it is not able to predict the system response to short-term or seasonal variations of boundary conditions. The separation of the sediment column into distinct biogeochemical zones and the resulting lack of overlap in degradation pathways may cause distorted organic matter degradation rates for the different TEAs. For instance, in OMEN-SED denitrification does not occur in the oxic layer, while in reality, although inhibited by the presence of oxygen, denitrification can still occur in the oxic zone, even at shallow sediments depths with high OM contents. Manganese and iron are not represented and as such OMEN-SED is not able to model all processes important in coastal marine environments and highly accumulating upwelling regions. This can cause problems when modelling H_2S and PO_4 profiles in anoxic environments as their concentrations are affected by these metal ions (compare Section 4.1). In addition the depth invariant porosity limits the correct calculation of the sediment-water interface flux of dissolved species as in reality porosity decreases with sediment depth.

6 Conclusions

In this paper we have described and tested a new, analytical early diagenetic model resolving organic matter cycling and associated biogeochemical dynamics called OMEN-SED. Our new model is the first of this class of analytical approaches to explicitly represent oxic degradation, denitrification, sulfate reduction and implicitly methanogenesis, as well as the re-oxidation of reduced substances produced during organic matter degradation. Pore water tracers include O_2, NO_3, NH_4, SO_4, H_2S,

DIC and ALK and the solid phase includes two fractions of organic matter, Fe-bound P and authigenic Ca-P minerals. We have shown that the new analytical model is able to reproduce observed pore water profiles from different ocean depths when organic matter partitioning and degradation rate constants are tuned to site specific conditions. An extensive sensitive analysis, based on the novel density-based PAWN method (Pianosi and Wagener, 2015), has been performed to asses the importance of 11 internal model parameters for all resulting SWI-fluxes. The results reveal that the degradation rate constant for labile organic matter is the most influential parameter for all model outputs. Under anoxic conditions secondary redox parameters exert an important control on related SWI-fluxes of SO_4, H_2S, NH_4 and alkalinity. In addition, the sensitivity analysis showed that globally observed benthic O_2 and NO_3 fluxes fall well into the range of produced model results.

Furthermore, the coupling of OMEN-SED to the Earth system model cGENIE is described and various published parameterisations for the apparent first order degradation rate constant are tested to fit the model to observed global organic matter concentrations. TODO: write about results. ...in order to investigate the role of sediments for global biogeochemical cycles and cimate.

7 Code Availability

The OMEN-SED source code (Fortran and MATLAB) related to this article is provided as a supplementary package together with a ReadMe file, where hardware and software requirements, source code files and model output file management are fully described.

Appendix A: Reaction Network

Appendix B: Sensitivity Analysis

B1

Acknowledgements. Thank you...

Table 15. Primary pathways of organic matter degradation, secondary redox reactions and stoichiometries implemented in the reaction network.

Pathway	Stoichiometry
	Primary Redox reactions
Aerobic degradation	$(CH_2O)_x(NH_3)_y(H_3PO_4)_z + (x+2y)O_2 + (y+2z)HCO_3^- \rightarrow (x+y+2z)CO_2 + yNO_3^- + zHPO_4^{2-} + (x+2y+2z)H_2O$
Denitrification	$(CH_2O)_x(NH_3)_y(H_3PO_4)_z + \frac{(4x+3y)}{5}NO_3^- \rightarrow \frac{(2x+4y)}{5}N_2 + \frac{(x-3y+10z)}{5}CO_2 + \frac{(4x+3y-10z)}{5}HCO_3^- + zHPO_4^{2-} + \frac{(3x+6y+10z)}{5}H_2O$
Sulfate reduction	$(CH_2O)_x(NH_3)_y(H_3PO_4)_z + \frac{x}{2}SO_4^{2-} + (y-2z)CO_2 + (y-2z)H_2O \rightarrow \frac{x}{2}H_2S + (x+y-2z)HCO_3^- + yNH_4^+ + zHPO_4^{2-}$
Methanogenesis	$(CH_2O)_x(NH_3)_y(H_3PO_4)_z + (y-2z)H_2O \rightarrow \frac{x}{2}CH_4 + \frac{x-2y+4z}{2}CO_2 + (x-2z)HCO_3^- + yNH_4^+ + zHPO_4^{2-}$
	Secondary Redox reactions
Nitrification	$NH_4^+ + 2O_2 + 2HCO_3^- \rightarrow NO_3^- + 2CO_2 + 3H_2O$
Sulfide oxidation	$H_2S + 2O_2 + 2HCO_3^- \rightarrow SO_4^{2-} + 2CO_2 + 2H_2O$
AOM	$CH_4 + CO_2 + SO_4^{2-} \rightarrow 2HCO_3^- + H_2S$
	Adsorption reactions and mineral precipitation
NH_4 adsorption	$NH_4^+ \xrightarrow{K_{NH_4}} NH_4^+(ads)$
P ad-/desorption ???	$PO_4^{2-} \xrightarrow{K_{PO_4}^{I,II}} PO_4^{2-}(ads)$; $HPO_4^{2-} \xrightarrow{k_s} Fe-bound\ P \xrightarrow{k_m} HPO_4^{2-}$
CFA precipitation	$PO_4^{2-} \xrightarrow{k_a} CFA$

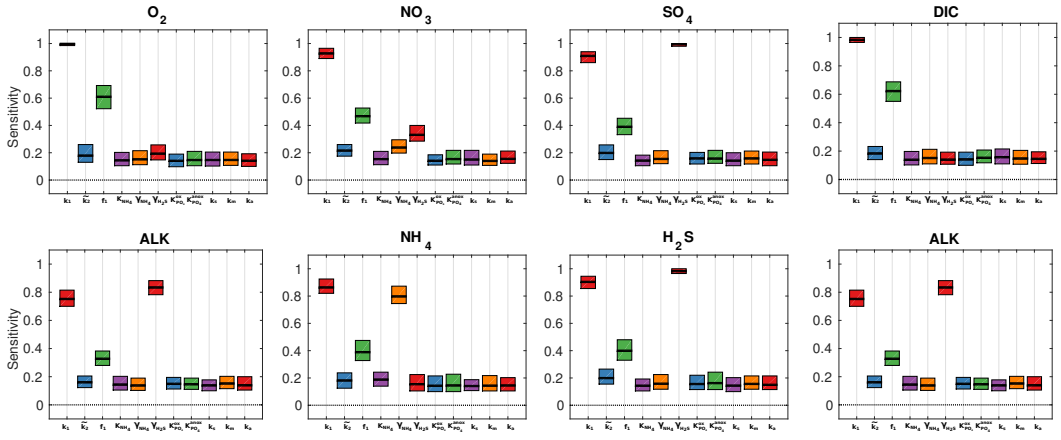

Figure 10. Move to Appendix Box plot of parameter sensitivities for the calculated SWI-fluxes for the 4000m oxic condition. Average sensitivities (black lines) and 90% confidence intervals using $N = 11200$ model evaluations and $Nboot = 100$ bootstrap resamples.

References

Aguilera, D. R., Jourabchi, P., Spiteri, C., and Regnier, P. (2005). A knowledge-based reactive transport approach for the simulation of biogeochemical dynamics in Earth systems. *Geochemistry, Geophysics, Geosystems*, 6(7).

Archer, D., Eby, M., Brovkin, V., Ridgwell, A., Cao, L., Mikolajewicz, U., Caldeira, K., Matsumoto, K., Munhoven, G., Montenegro, A., and Tokos, K. (2009). Atmospheric Lifetime of Fossil Fuel Carbon Dioxide. *Annual Review of Earth and Planetary Sciences*, 37(1):117–134.

Archer, D. and Maier-Reimer, E. (1994). Effect of Deep-Sea Sedimentary Calcite Preservation on Atmospheric Co2 Concentration. *Nature*, 367(6460):260–263. 00506 WOS:A1994MR49400052.

Archer, D., Winguth, A., Lea, D., and Mahowald, N. (2000). What caused the glacial/interglacial atmospheric pCO2 cycles? *Reviews of Geophysics*, 38(2):159–189. 00414.

Archer, D. E., Morford, J. L., and Emerson, S. R. (2002). A model of suboxic sedimentary diagenesis suitable for automatic tuning and gridded global domains. *Global Biogeochemical Cycles*, 16(1):17–1.

Arndt, S., Jørgensen, B., LaRowe, D., Middelburg, J., Pancost, R., and Regnier, P. (2013). Quantifying the degradation of organic matter in marine sediments: A review and synthesis. *Earth-Science Reviews*, 123:53–86.

Arthur, M. A., Dean, W. E., and Pratt, L. M. (1988). Geochemical and climatic effects of increased marine organic carbon burial at the Cenomanian/Turonian boundary. *Nature*, 335(6192):714–717.

Berner, R. A. (1980). *Early Diagenesis: A Theoretical Approach*. Princeton University Press.

Berner, R. A. (1991). A model for atmospheric CO_2 over Phanerozoic time. 291(4):339–376.

Berner, R. A. (2004). *The Phanerozoic Carbon Cycle: CO2 and O2*. Oxford University Press. 00000.

Bohlen, L., Dale, A. W., and Wallmann, K. (2012). Simple transfer functions for calculating benthic fixed nitrogen losses and C:N:P regeneration ratios in global biogeochemical models. *Global Biogeochemical Cycles*, 26(3):GB3029.

Boudreau, B. P. (1996). A method-of-lines code for carbon and nutrient diagenesis in aquatic sediments. *Computers & Geosciences*, 22(5):479–496.

Boudreau, B. P. (1997). *Diagenetic models and their implementation*, volume 505. Springer Berlin.

Boudreau, B. P. (1998). Mean mixed depth of sediments: The wherefore and the why. *Limnology and Oceanography*, 43(3):524–526.

Boudreau, B. P., Mucci, A., Sundby, B., Luther, G. W., and Silverberg, N. (1998). Comparative diagenesis at three sites on the Canadian continental margin. *Journal of Marine Research*, 56(6):1259–1284.

Boudreau, B. P. and Ruddick, B. R. (1991). On a reactive continuum representation of organic matter diagenesis. *American Journal of Science*, 291(5):507–538. 00187.

Broecker, W. S. (1982). Ocean chemistry during glacial time. *Geochimica et Cosmochimica Acta*, 46(10):1689–1705.

Burdige, D. J. (2006). *Geochemistry of marine sediments*, volume 398. Princeton University Press Princeton.

Canfield, D. E., Kristensen, E., and Thamdrup, B. (2005). *Aquatic Geomicrobiology*. Gulf Professional Publishing.

Canfield, D. E. and Thamdrup, B. (2009). Towards a consistent classification scheme for geochemical environments, or, why we wish the term 'suboxic' would go away. *Geobiology*, 7(4):385–392.

Colbourn, G., Ridgwell, A., and Lenton, T. M. (2013). The Rock Geochemical Model (RokGeM) v0.9. *Geosci. Model Dev.*, 6(5):1543–1573.

Edwards, N. R. and Marsh, R. (2005). Uncertainties due to transport-parameter sensitivity in an efficient 3-D ocean-climate model. *Climate Dynamics*, 24(4):415–433.

Emerson, S. and Bender, M. L. (1981). Carbon fluxes at the sediment-water interface of the deep-sea: calcium carbonate preservation. *Journal of Marine Research*, 39:139–162.

Epping, E., van der Zee, C., Soetaert, K., and Helder, W. (2002). On the oxidation and burial of organic carbon in sediments of the Iberian margin and Nazaré Canyon (NE Atlantic). *Progress in Oceanography*, 52(2–4):399–431.

Goosse, H., Brovkin, V., Fichefet, T., Haarsma, R., Huybrechts, P., Jongma, J., Mouchet, A., Selten, F., Barriat, P.-Y., Campin, J.-M., Deleersnijder, E., Driesschaert, E., Goelzer, H., Janssens, I., Loutre, M.-F., Morales Maqueda, M. A., Opsteegh, T., Mathieu, P.-P., Munhoven, G., Pettersson, E. J., Renssen, H., Roche, D. M., Schaeffer, M., Tartinville, B., Timmermann, A., and Weber, S. L. (2010). Description of the earth system model of intermediate complexity LOVECLIM version 1.2. *Geosci. Model Dev.*, 3(2):603–633.

Gypens, N., Lancelot, C., and Soetaert, K. (2008). Simple parameterisations for describing n and p diagenetic processes: Application in the north sea. *Progress in Oceanography*, 76(1):89–110.

Heinze, C., Maier-Reimer, E., Winguth, A. M. E., and Archer, D. (1999). A global oceanic sediment model for long-term climate studies. *Global Biogeochemical Cycles*, 13(1):221–250.

Hensen, C., Zabel, M., and Schulz, H. N. (2006). Benthic Cycling of Oxygen, Nitrogen and Phosphorus. In Schulz, H. D. and Zabel, M., editors, *Marine Geochemistry*, pages 207–240. Springer Berlin Heidelberg.

Hülse, D., Arndt, S., Wilson, J., Munhoven, G., and Ridgwell, A. (2017). Understanding the causes and consequences of past marine carbon cycling variability through models. *Earth-Science Reviews*, –:in review.

Ilyina, T., Six, K. D., Segschneider, J., Maier-Reimer, E., Li, H., and Núñez-Riboni, I. (2013). Global ocean biogeochemistry model HAMOCC: Model architecture and performance as component of the MPI-Earth system model in different CMIP5 experimental realizations. *Journal of Advances in Modeling Earth Systems*, 5(2):287–315.

Ingall, E. and Jahnke, R. (1994). Evidence for enhanced phosphorus regeneration from marine sediments overlain by oxygen depleted waters. *Geochimica et Cosmochimica Acta*, 58(11):2571–2575. 00302.

Jarvis, I., Lignum, J. S., Gröcke, D. R., Jenkyns, H. C., and Pearce, M. A. (2011). Black shale deposition, atmospheric CO2 drawdown, and cooling during the Cenomanian-Turonian Oceanic Anoxic Event. *Paleoceanography*, 26(3):n/a–n/a.

Jenkyns, H. C. (2010). Geochemistry of oceanic anoxic events. *Geochemistry, Geophysics, Geosystems*, 11(3).

Jørgensen, B. B. (1978). A comparison of methods for the quantification of bacterial sulfate reduction in coastal marine sediments: II Calculation from mathematical models. *Geomicrobiology Journal*, 1:29–47.

Jørgensen, B. B. and Kasten, S. (2006). Sulfur Cycling and Methane Oxidation. In Schulz, P. D. H. D. and Zabel, D. M., editors, *Marine Geochemistry*, pages 271–309. Springer Berlin Heidelberg.

Krom, M. D. and Berner, R. A. (1980). Adsorption of phosphate in anoxic marine sediments1. *Limnology and Oceanography*, 25(5):797–806.

Lenton, T. M. and Watson, A. J. (2000). Redfield revisited: 1. Regulation of nitrate, phosphate, and oxygen in the ocean. *Global Biogeochemical Cycles*, 14(1):225–248.

Li, Y.-H. and Gregory, S. (1974). Diffusion of ions in sea water and in deep-sea sediments. *Geochimica et Cosmochimica Acta*, 38(5):703–714.

Mackenzie, F. T. (2005). *Sediments, Diagenesis, and Sedimentary Rocks: Treatise on Geochemistry, Second Edition*. Elsevier. 00000.

Meysman, F. J. R., Middelburg, J. J., Herman, P. M. J., and Heip, C. H. R. (2003). Reactive transport in surface sediments. II. Media: an object-oriented problem-solving environment for early diagenesis. *Computers & Geosciences*, 29(3):301–318. 00067.

Middelburg, J. J., Soetaert, K., and Herman, P. M. (1997). Empirical relationships for use in global diagenetic models. *Deep Sea Research Part I: Oceanographic Research Papers*, 44(2):327–344.

Middelburg, J. J., Soetaert, K., Herman, P. M. J., and Heip, C. H. R. (1996). Denitrification in marine sediments: A model study. *Global Biogeochemical Cycles*, 10(4):661–673.

Mort, H. P., Adatte, T., Föllmi, K. B., Keller, G., Steinmann, P., Matera, V., Berner, Z., and Stüben, D. (2007). Phosphorus and the roles of productivity and nutrient recycling during oceanic anoxic event 2. *Geology*, 35(6):483–486. 00135.

Munhoven, G. (2007). Glacial–interglacial rain ratio changes: Implications for atmospheric and ocean–sediment interaction. *Deep Sea Research Part II: Topical Studies in Oceanography*, 54(5–7):722–746.

Najjar, R. G., Jin, X., Louanchi, F., Aumont, O., Caldeira, K., Doney, S. C., Dutay, J.-C., Follows, M., Gruber, N., Joos, F., Lindsay, K., Maier-Reimer, E., Matear, R. J., Matsumoto, K., Monfray, P., Mouchet, A., Orr, J. C., Plattner, G.-K., Sarmiento, J. L., Schlitzer, R., Slater, R. D., Weirig, M.-F., Yamanaka, Y., and Yool, A.

(2007). Impact of circulation on export production, dissolved organic matter, and dissolved oxygen in the ocean: Results from Phase II of the Ocean Carbon-cycle Model Intercomparison Project (OCMIP-2). *Global Biogeochemical Cycles*, 21(3):GB3007.

Palastanga, V., Slomp, C. P., and Heinze, C. (2011). Long-term controls on ocean phosphorus and oxygen in a global biogeochemical model. *Global Biogeochemical Cycles*, 25(3):GB3024.

Pianosi, F., Beven, K., Freer, J., Hall, J. W., Rougier, J., Stephenson, D. B., and Wagener, T. (2016). Sensitivity analysis of environmental models: A systematic review with practical workflow. *Environmental Modelling & Software*, 79:214–232.

Pianosi, F., Sarrazin, F., and Wagener, T. (2015). A Matlab toolbox for Global Sensitivity Analysis. *Environmental Modelling & Software*, 70:80–85.

Pianosi, F. and Wagener, T. (2015). A simple and efficient method for global sensitivity analysis based on cumulative distribution functions. *Environmental Modelling & Software*, 67:1–11.

Reimers, C. E., Ruttenberg, K. C., Canfield, D. E., Christiansen, M. B., and Martin, J. B. (1996). Porewater pH and authigenic phases formed in the uppermost sediments of the Santa Barbara Basin. *Geochimica et Cosmochimica Acta*, 60(21):4037–4057.

Ridgwell, A. and Hargreaves, J. C. (2007). Regulation of atmospheric CO2 by deep-sea sediments in an Earth system model. *Global Biogeochemical Cycles*, 21(2):n/a–n/a.

Ridgwell, A., Hargreaves, J. C., Edwards, N. R., Annan, J. D., Lenton, T. M., Marsh, R., Yool, A., and Watson, A. (2007). Marine geochemical data assimilation in an efficient Earth System Model of global biogeochemical cycling. *Biogeosciences*, 4(1):87–104. 00090.

Ridgwell, A. and Zeebe, R. E. (2005). The role of the global carbonate cycle in the regulation and evolution of the Earth system. *Earth and Planetary Science Letters*, 234(3–4):299–315. 00172.

Ruttenberg, K. C. (1993). Reassessment of the oceanic residence time of phosphorus. *Chemical Geology*, 107(3):405–409.

Schulz, H. D. (2006). Quantification of Early Diagenesis: Dissolved Constituents in Pore Water and Signals in the Solid Phase. In Schulz, P. D. H. D. and Zabel, D. M., editors, *Marine Geochemistry*, pages 73–124. Springer Berlin Heidelberg.

Shaffer, G., Malskær Olsen, S., and Pepke Pedersen, J. O. (2008). Presentation, calibration and validation of the low-order, DCESS Earth System Model (Version 1). *Geosci. Model Dev.*, 1(1):17–51. 00007.

Slomp, C., Malschaert, J., and Van Raaphorst, W. (1998). The role of adsorption in sediment-water exchange of phosphate in north sea continental margin sediments. *Limnology and Oceanography*, 43(5):832–846.

Slomp, C. P., Epping, E. H., Helder, W., and Van Raaphorst, W. (1996). A key role for iron-bound phosphorus in authigenic apatite formation in north atlantic continental platform sediments. *Journal of Marine Research*, 54(6):1179–1205.

Soetaert, K., Herman, P. M., and Middelburg, J. J. (1996a). Dynamic response of deep-sea sediments to seasonal variations: a model. *Limnology and Oceanography*, 41(8):1651–1668.

Soetaert, K., Herman, P. M. J., and Middelburg, J. J. (1996b). A model of early diagenetic processes from the shelf to abyssal depths. *Geochimica et Cosmochimica Acta*, 60(6):1019–1040.

Soetaert, K., Middelburg, J. J., Herman, P. M. J., and Buis, K. (2000). On the coupling of benthic and pelagic biogeochemical models. *Earth-Science Reviews*, 51(1–4):173–201.

Stein, R., Rullkötter, J., and Welte, D. H. (1986). Accumulation of organic-carbon-rich sediments in the Late Jurassic and Cretaceous Atlantic Ocean — A synthesis. *Chemical Geology*, 56(1–2):1–32.

Stolpovsky, K., Dale, A. W., and Wallmann, K. (2015). Toward a parameterization of global-scale organic carbon mineralization kinetics in surface marine sediments. *Global Biogeochemical Cycles*, 29(6):2015GB005087.

Stumm, W. and Morgan, J. J. (2012). *Aquatic Chemistry: Chemical Equilibria and Rates in Natural Waters*. John Wiley & Sons.

Teal, L., Bulling, M., Parker, E., and Solan, M. (2010). Global patterns of bioturbation intensity and mixed depth of marine soft sediments. *Aquatic Biology*, 2(3):207–218.

Thullner, M., Dale, A. W., and Regnier, P. (2009). Global-scale quantification of mineralization pathways in marine sediments: A reaction-transport modeling approach. *Geochemistry, Geophysics, Geosystems*, 10(10).

Tjiputra, J. F., Roelandt, C., Bentsen, M., Lawrence, D. M., Lorentzen, T., Schwinger, J., Seland, Ø., and Heinze, C. (2013). Evaluation of the carbon cycle components in the Norwegian Earth System Model (NorESM). *Geosci. Model Dev.*, 6(2):301–325. 00057.

Toth, D. J. and Lerman, A. (1977). Organic matter reactivity and sedimentation rates in the ocean. *American Journal of Science*, 277(4):465–485.

Tromp, T. K., Van Cappellen, P., and Key, R. M. (1995). A global model for the early diagenesis of organic carbon and organic phosphorus in marine sediments. *Geochimica et Cosmochimica Acta*, 59(7):1259–1284. 00164.

Tsandev, I. and Slomp, C. (2009). Modeling phosphorus cycling and carbon burial during Cretaceous Oceanic Anoxic Events. *Earth and Planetary Science Letters*, 286(1–2):71–79.

Ullman, W. J. and Aller, R. C. (1982). Diffusion coefficients in nearshore marine sediments. *Limnology and Oceanography*, 27(3):552–556.

Van Cappellen, P. and Berner, R. A. (1988). A mathematical model for the early diagenesis of phosphorus and fluorine in marine sediments; apatite precipitation. *American Journal of Science*, 288(4):289–333.

Van Cappellen, P. and Ingall, E. D. (1994). Benthic phosphorus regeneration, net primary production, and ocean anoxia: A model of the coupled marine biogeochemical cycles of carbon and phosphorus. *Paleoceanography*, 9(5):677–692.

Van Cappellen, P. and Wang, Y. (1996). Cycling of iron and manganese in surface sediments; a general theory for the coupled transport and reaction of carbon, oxygen, nitrogen, sulfur, iron, and manganese. *American Journal of Science*, 296(3):197–243.

Wang, Y. and Van Cappellen, P. (1996). A multicomponent reactive transport model of early diagenesis: Application to redox cycling in coastal marine sediments. *Geochimica et Cosmochimica Acta*, 60(16):2993–3014. 00283.

Wolf-Gladrow, D. A., Zeebe, R. E., Klaas, C., Körtzinger, A., and Dickson, A. G. (2007). Total alkalinity: The explicit conservative expression and its application to biogeochemical processes. *Marine Chemistry*, 106(1–2):287–300.